Deep-Sea Research II 58 (2011) 1075–1091

Contents lists available at ScienceDirect

Deep-Sea Research II

journal homepage: www.elsevier.com/locate/dsr2

The characteristics of dissolved organic matter (DOM) and chromophoric dissolved organic matter (CDOM) in Antarctic sea ice

Louiza Norman [a], David N. Thomas [a,*], Colin A. Stedmon [b], Mats A. Granskog [c,d], Stathys Papadimitriou [a], Rupert H. Krapp [e], Klaus M. Meiners [f], Delphine Lannuzel [f,g], Pier van der Merwe [f,h], Gerhard S. Dieckmann [i]

[a] School of Ocean Sciences, College of Natural Sciences, Bangor University, Menai Bridge, Anglesey LL59 5AB, UK
[b] Department of Marine Ecology, National Environmental Research Institute, Aarhus University, Frederiksborgvej 399, 4000 Roskilde, Denmark
[c] Arctic Centre, University of Lapland, 96101 Rovaniemi, Finland
[d] Norwegian Polar Institute, Polar Environmental Centre, 9296 Tromsø, Norway
[e] University Center in Svalbard, P.O. Box 156, N-9171 Longyearbyen, Norway
[f] Antarctic Climate and Ecosystems Cooperative Research Centre, Private Bag 80, Hobart 7001, Tasmania, Australia
[g] Centre for Marine Science, Private Bag 78, Hobart, Tasmania 7001, Australia
[h] Institute of Antarctic and Southern Ocean Studies, University of Tasmania, Private Bag 50, Hobart, Tasmania 7001, Australia
[i] Alfred Wegener Institute for Polar and Marine Research, Am Handelshafen 12, D-27570 Bremerhaven, Germany

ARTICLE INFO

Article history:
Received 20 October 2010
Accepted 20 October 2010
Available online 7 January 2011

Keywords:
Sea ice
Antarctic
Coloured dissolved organic matter (CDOM)
Dissolved organic matter (DOM)
Photochemistry
Biogeochemistry

ABSTRACT

An investigation of coloured dissolved organic matter (CDOM) and its relationships to physical and biogeochemical parameters in Antarctic sea ice and oceanic water have indicated that ice melt may both alter the spectral characteristics of CDOM in Antarctic surface waters and serve as a likely source of fresh autochthonous CDOM and labile DOC. Samples were collected from melted bulk sea ice, sea ice brines, surface gap layer waters, and seawater during three expeditions: one during the spring to summer and two during the winter to spring transition period. Variability in both physical (temperature and salinity) and biogeochemical parameters (dissolved and particulate organic carbon and nitrogen, as well as chlorophyll *a*) was observed during and between studies, but CDOM absorption coefficients measured at 375 nm (a_{375}) did not differ significantly. Distinct peaked absorption spectra were consistently observed for bulk ice, brine, and gap water, but were absent in the seawater samples. Correlation with the measured physical and biogeochemical parameters could not resolve the source of these peaks, but the shoulders and peaks observed between 260 and 280 nm and between 320 to 330 nm respectively, particularly in the samples taken from high light-exposed gap layer environment, suggest a possible link to aromatic and mycosporine-like amino acids. Sea ice CDOM susceptibility to photo-bleaching was demonstrated in an *in situ* 120 hour exposure, during which we observed a loss in CDOM absorption of 53% at 280 nm, 58% at 330 nm, and 30% at 375 nm. No overall coincidental loss of DOC or DON was measured during the experimental period. A relationship between the spectral slope (S) and carbon-specific absorption (a^*_{375}) indicated that the characteristics of CDOM can be described by the mixing of two broad end-members; and aged material, present in brine and seawater samples characterised by high S values and low a^*_{375}; and a fresh material, due to elevated *in situ* production, present in the bulk ice samples characterised by low S and high a^*_{375}. The DOC data reported here have been used to estimate that approximately 8 Tg C yr^{-1} ($\sim$11% of annual sea ice algae primary production) may be exported to the surface ocean during seasonal sea ice melt in the form of DOC.

1. Introduction

Sea ice in the polar oceans (Arctic and Southern) and sub-polar seas (e.g., Baltic and White Seas, Hudson Bay) provides a range of physically and geochemically unique habitats, which can support rich and diverse biological assemblages. Sea ice has long been recognised to play a key role in the biogeochemical cycles of ice-covered oceans and seas (Thomas and Dieckmann, 2002a, b; Thomas et al., 2010). The biogeochemical composition of sea ice often yields elevated concentrations of dissolved organic matter (DOM) (Thomas et al., 2010) with distinct optical characteristics as determined on the coloured fraction

* Corresponding author. Tel./fax: +44 1248 382 878.
E-mail addresses: Louisa.Norman@student.uts.edu.au (L. Norman), d.thomas@bangor.ac.uk (D.N. Thomas), cst@dmu.dk (C.A. Stedmon), mats.granskog@npolar.no (M.A. Granskog), s.papadimitriou@bangor.ac.uk (S. Papadimitriou), rkrapp@gmail.com (R.H. Krapp), Klaus.Meiners@acecrc.org.au (K.M. Meiners), delphine.lannuzel@utas.edu.au (D. Lannuzel), pvander@utas.edu.au (P. van der Merwe), Gerhard.dieckmann@awi.de (G.S. Dieckmann).

0967-0645/$ - see front matter © 2010 Elsevier Ltd. All rights reserved.
doi:10.1016/j.dsr2.2010.10.030

of DOM, chromophoric dissolved organic matter (CDOM), relative to the surrounding surface waters (Perovich et al., 1998; Belzile et al., 2000; Stedmon et al., 2007).

The marine DOM pool consists of both allochthonous (terrestrial) and autochthonous (marine) material derived from the biosynthesis of organic matter (Nelson and Siegel, 2002). Ubiquitous in all marine environments, CDOM can make up a substantial proportion of the DOM pool in aquatic systems (Thurman, 1985; Coble, 2007), representing up to 60% of the bulk DOC pool (Ertel et al., 1986). The reactivity of CDOM to sunlight has a significant effect on the cycling of both DOM and CDOM (Obernosterer and Benner, 2004) as the absorption of UV radiation by CDOM initiates a set of photochemical reactions, which either directly remineralise the organic matter or leads to the formation of a number of reactive products (Miller and Zepp, 1995; Uher and Andreae, 1997; King et al., 2005; Stubbins et al., 2006; Xie et al., 2009) some of which (i.e. ammonium and phosphate) are biologically labile (Moran and Zepp, 1997; Kitidis et al., 2008).

The optical characteristics of sea ice CDOM are a composite of those of the CDOM present in the surface oceanic water, from which the ice formed, and those of the CDOM in the DOM pool produced in sea ice by the activity of sympagic organisms (Thomas et al., 2001; Granskog et al., 2006; Stedmon et al., 2007). The *in situ* DOM production and its cycling in the often closed environment of sea ice, with little or intermittent accessibility to the pool of nutrients in the surface ocean, can be an important source of nutrients to sympagic assemblages.

One of the unique features of the seasonally ice-covered region of the Southern Ocean is that there are no major terrestrial inputs of DOM, which is in stark contrast to the northern polar and sub-polar regions that are influenced by dense and large river networks (Retamal et al., 2007). Hence, the DOM incorporated in Arctic and sub-Arctic sea ice during ice formation has a substantial river-borne allochthonous component (Benner et al., 2005; Granskog et al., 2006; Stedmon et al., 2007), whereas the DOM incorporated into sea ice formed in the Southern Ocean will be predominantly autochthonous in origin. As a result, the Southern Ocean provides a unique opportunity to investigate the composition and behavior of marine-derived organic matter divorced from terrestrial inputs.

There are very few studies of the optical characteristics of CDOM in sea ice, with none, to our knowledge, in Antarctic sea ice. As mentioned above, the optical properties of CDOM in Baltic sea ice have been shown to differ from that of the under-ice seawater (Ehn et al., 2004; Granskog et al., 2005) as a result of *in situ* (sympagic) CDOM production (Stedmon et al., 2007). Belzile et al. (2000) showed that CDOM was a significant component of the DOM pool attenuating UV light in Arctic first-year sea ice, as did Ehn et al. (2004) and Uusikivi et al. (2010) for the Baltic Sea. Scully and Miller (2000) concluded that melting sea ice would be a source of CDOM to the surface ocean in Baffin Bay (Canadian Arctic), and both Kieber et al. (2009) and Ortega-Retuerta et al. (2010) considered that Antarctic sea ice might be a potential source of CDOM, although this was suggested without direct evidence. The limited number of polar and sub-polar studies have revealed the potential of sea ice as a CDOM reactor and a source of CDOM with distinct optical properties to the surface ocean.

In this study we investigated the optical properties of CDOM in Antarctic sea ice from two regions of the polar Southern Ocean, the Weddell Sea and East Antarctica, in the early spring and early summer. The data were collected from a wide range of sea ice types in respect of age, temperature, and thickness, as well as biological standing stocks. We report on the optical properties of CDOM from directly-sampled sea ice brine, melted (bulk) sea ice from ice cores, the hyposaline water from surface gap layers, and seawater. The relationships between the spectral properties of CDOM and the concentrations of DOC, dissolved organic nitrogen (DON), particulate organic carbon (POC), particulate nitrogen (PN), and chlorophyll *a* (Chl*a*) are examined and discussed in relation to the importance of CDOM in the sea ice, and we assess the potential of sea ice as a source of CDOM to the Southern Ocean.

2. Study sites and sampling

2.1. Study sites

The initial part of the study was conducted in the transition from spring to summer (December 2004) during the interdisciplinary field experiment *Ice Station POLarstern* (ISPOL) (Hellmer et al., 2008). During the experiment, the physical and biogeochemical properties of a single, 10 × 10 km (initial dimensions) ice floe were monitored. The ISPOL floe was located in the western Weddell Sea, where it drifted in a northerly direction at approximately 67–68°S and 55°W (Fig. 1). Samples were taken from first- and second-year ice from the structurally heterogeneous ISPOL floe, as well as from the water of 2 spatially separate gap layers in the upper 10 to 30 cm of the ice column. Details of the physical and chemical features of the floe have been reported elsewhere (Haas et al., 2007; Lannuzel et al., 2008; Papadimitriou et al., 2007, 2009).

The second part of the study was conducted in the transition from winter to spring (September–October 2006) during the *Winter Weddell Outflow Study* (WWOS) on board R.V. *Polarstern* (Lemke, 2009). The cruise track took an east to west transect between 60° to 61°S and 40° to 52°W, and a northeast to southwest transect between 60°S and 65°S, in the north-western Weddell Sea (Hellmer et al., 2009). Brine and ice core samples were obtained at 22 ice stations during a 38-day period (Fig. 1). Physical, chemical, and biological parameters of the WWOS sites have been reported in Haas et al. (2009) and Meiners et al. (2009).

The third part of the study was conducted during the *Sea Ice Physics and Ecosystem Experiment* (SIPEX) onboard the R.S. *Aurora Australis* in the transition from winter to spring (September–October 2007) on 14 ice stations within the 110–130° E region off Eastern Antarctica (Fig. 1). During the SIPEX experiment, the sea ice was thinner than that studied during ISPOL and WWOS, with many of the floes relatively undeformed and less than 60 cm thick. The majority of samples were taken from first-year ice. One station was fast ice, and one station was rafted consolidated pancake sea ice close to the marginal ice zone from which two cores were taken.

2.2. Sampling

Under-ice seawater samples were taken using a Seabird 911+CTD rosette equipped with 12 L Niskin bottles during ISPOL and WWOS, and with a manual, messenger-operated 2 L Niskin bottle during SIPEX. All samples were collected in acid-cleaned 1 or 2 L HDPE bottles.

Ice cores were drilled either manually or using an electric motor, using a KOVACS Mark II (9 cm internal diameter) ice corer, and were immediately sectioned into 10 cm segments directly into acid-cleaned 1L plastic tubs. To maintain consistency all cores were sectioned starting at the bottom of the core and working towards the top. Temperature measurements were taken from a companion core by drilling a small hole at the mid-point of each 10 cm section and inserting a calibrated K–Thermocouple probe on a HANNA Instruments thermometer (HI93530). All ice core sections were then returned to the onboard laboratory and were melted in the dark at +4 °C.

Brine samples were collected using the sackhole sampling method by manually drilling partial bore holes into the ice surface after removing the snow cover and allowing the brine from the surrounding brine channels to percolate into the hole (Gleitz et al., 1995). Between three and six sackholes were drilled on each

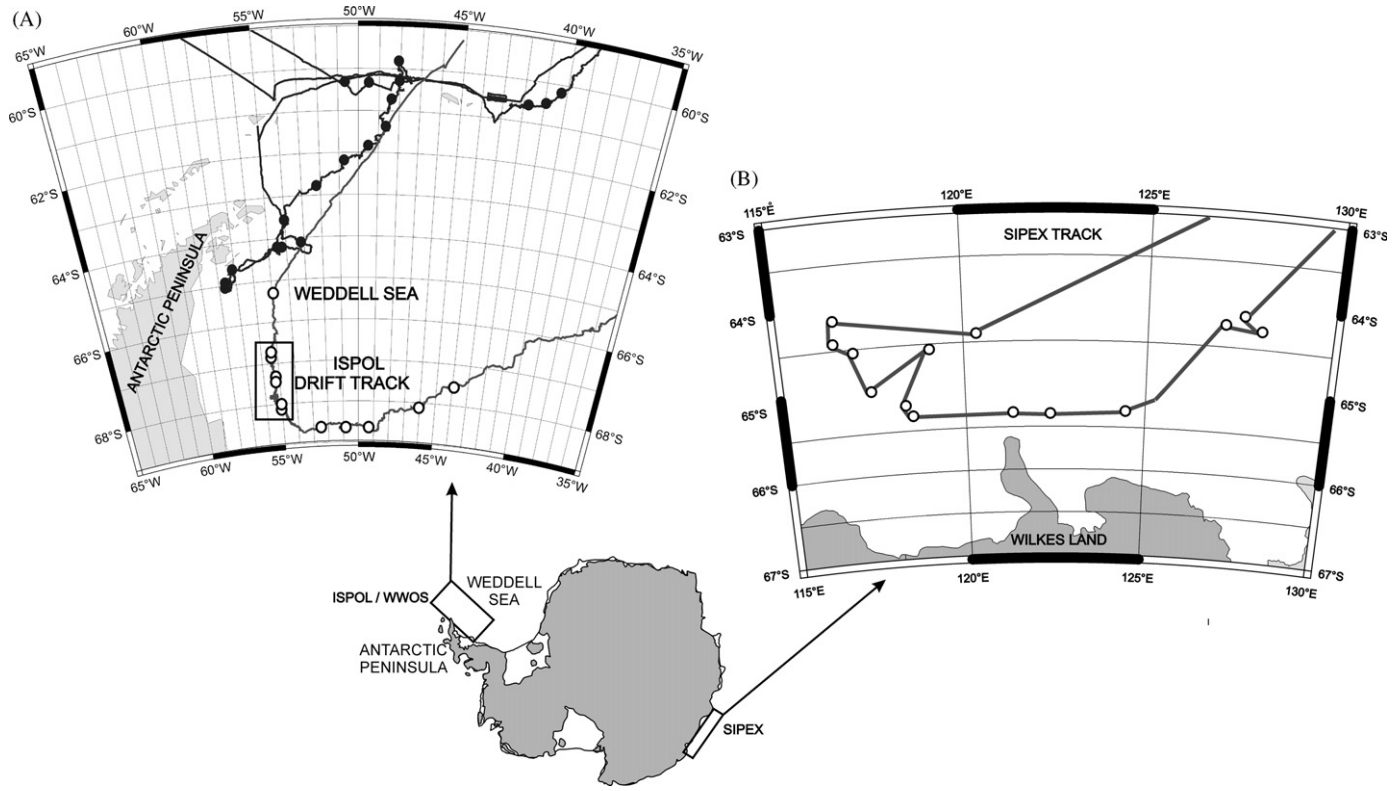

Fig. 1. Cruise tracks and ice stations for (A) the ISPOL drift experiment (27/11/04 to 02/01/05), indicated with open circles, with drift area contained within box, and the WWOS field study (06/09/06 to 13/10/06), indicated with solid circles, both in the Weddell Sea, Antarctica, and (B) the SIPEX field study (11/09/07 to 10/10/07) in the Eastern Antarctic region. The ISPOL/WWOS map was provided by Marcel Nicolaus, Norwegian Polar Institute. The SIPEX map was generated using Online Map Creation.

occasion using a 14 cm (ID) Kovacs Mark V ice corer within approximately a 2 m^2 ice surface to depths between 16 and 186 cm, but mostly in the 30 to 60 cm range, depending on the thickness of the ice. Ice shavings and slush were removed, and Styrofoam covers were placed over the top of the sackholes to ensure that samples were not compromised by snow, slush, or debris, and to minimise air-brine interaction (Papadimitriou et al., 2007). During ISPOL, sufficient volume of brine was generally collected after 10 minutes, but due to the colder temperatures during the WWOS and SIPEX studies, the time required to collect sufficient brine was 0.5 to 3, and 3 to 7 hours, respectively. The brine samples were collected into acid-cleaned 1L plastic containers using an acid-cleaned 100 mL plastic syringe fitted with a 30 cm length of Teflon tubing. Deeper sackholes were sampled with a stainless steel ladle attached to a pole. The brine temperature was measured *in situ* using a calibrated K–Thermocouple probe on a HANNA Instruments thermometer (HI93530). Sackhole sampling has been shown to be a suitable method for measurements of dissolved constituents in brines but unsuitable for quantitative measurements of the particulate fraction because the latter does not percolate quantitatively with the brine (Weissenberger, 1992; Papadimitriou et al., 2007). The concentrations of Chl*a*, POC, and PN measured in sackhole brine samples are therefore underestimates of actual *in situ* concentrations and are reported here only as relative abundance indicators for biomass.

2.3. Samples

The ISPOL samples comprised:

1) Seawater samples from four CTD stations at water depths between 5 and 1516 m;
2) Seven ice cores from two sites on the floe, five ice cores from a level 50 × 50 m patch of thin first-year ice, and two ice cores from a spatially separate site with thick second-year ice;
3) 31 brine samples, 28 hypersaline (salinity > 35) and 3 hyposaline (salinity < 35), 29 from a separate site on the floe with thick first-year ice and two from a location with thick second-year ice;
4) 23 hyposaline water samples from two spatially separate gap layers, one overlying thick first-year ice and another overlying second-year ice from which the two ice cores were also obtained as described in 2) above.

The five ice cores from the thin first-year ice described in 2) above were part of a temporal study and were taken at approximately 5 day intervals between 29/11/04 and 30/12/04. The brine samples were collected between 02/12/04 and 29/12/04 at intervals of 3 to 9 days, with a minimum of three sackholes sampled at each sampling event. The biological and geochemical composition of the hypersaline sackhole brines and the hyposaline gap waters from the ISPOL floe has been reported in Papadimitriou et al. (2007, 2009).

The WWOS samples comprised:

1) Seawater samples from five CTD stations at water depths between 20 and 5591 m;
2) 12 ice cores, 11 from first-year ice and one from second-year ice;
3) 118 brine samples, 100 from first-year ice and 18 from second-year ice.

The SIPEX samples comprised:

1) 28 under-ice water samples taken at between 1 and 10 m depth;
2) 33 ice cores, 30 from first-year ice and three from second-year ice;

3) 38 brine samples, 33 from first-year ice and five from second-year ice.

Fifteen of the ice cores and 16 of the brine samples were taken from sites dedicated to trace iron analysis (van der Merwe et al., 2009). One core was taken from a heavily deformed floe (209 cm thick), and one further core and three brine samples came from an area of land fast ice.

2.4. Photo-bleaching experiment

In addition to field sampling, a CDOM photo-bleaching experiment was set up during ISPOL in order to investigate the changes in brine CDOM during photo-bleaching at *in situ* conditions. Ten borosilicate and 10 quartz 220-mL tubes with stoppers (all pre-combusted at 500 °C for 3 hours) were filled with filtered (using pre-combusted WHATMAN GF/F filters) brine taken from a single sackhole (salinity=55.2). The borosilicate tubes were wrapped in foil to maintain dark conditions and served as control samples, while the quartz tubes were left unwrapped. All vessels were then half-buried in surface snow to minimise temperature variation. Samples for CDOM, DOC, and DON analyses were taken at time zero. Thereafter, two control tubes and two experimental tubes were harvested, thoroughly mixed, and sampled for CDOM, DOC, and DON analyses at 12, 18, 24, 48, and 120 hours. During the experiment light measurements were recorded using a hyperspectral radiometer (TriOS RAMSES ACC-UV) for the UVA (measured between 320 and 400 nm) and UVB (measured between 280 and 320 nm) spectral range, while 2π quantum sensor (LI-190) was used for the PAR range (400 to 550 nm). Both sensors were placed on the snow surface in proximity to the sample vials, making sure that no shading effects occurred by any of the sensors, cables or connected recorders. The sensors were connected to a PC and a LI-COR datalogger (LI-1400) for control and data storage, respectively. The sampling rates were set to 5 min intervals and the spectral resolution for the radiometer was 2.2 nm. The PAR data are expressed in $\mu mol\ m^{-2}\ s^{-1}$ while the UVR data are expressed in $W\ m^{-2}$.

2.5. Analytical techniques

All salinity measurements were taken at laboratory temperature (17 to 22 °C) using a SEMAT Cond 315i/SET salinometer with WTW Tetracon 325 probe. As the maximum range of the instrument is salinity=70 (measured in PSU), samples with higher salinity were measured after dilution with ultrapure water. The samples for the determination of Chl*a*, POC, and PN were collected from an aliquot of known volume on pre-combusted (500 °C, three hours) filters (WHATMAN, GF/F) and were kept at −20 °C until analysis of Chl*a* in the onboard laboratory and POC/PN in the Bangor University (ISPOL and WWOS) and University of Tasmania (SIPEX) laboratories. The extracted Chl*a* was measured using a Turner Designs 10 AU fluorometer (detection limit of the instrument 0.02 $\mu g\ L^{-1}$) following the method of Evans et al. (1987) during ISPOL and WWOS, and Holm-Hansen et al. (1965) during SIPEX. The POC and PN concentrations were determined with a CARLO ERBA NA 1500 Elemental CHN Analyzer (ISPOL and WWOS) and a Thermo Finnigan EA 1112 Series Flash Elemental Analyser (SIPEX) after overnight fumigation with 37% (w/v) HCl to remove the inorganic carbon fraction and oven-drying at 60 °C.

The filtrate provided samples for DOC, DON, and CDOM measurements during ISPOL and WWOS, while, during SIPEX, such samples were obtained by filtering through disposable syringe filters (WHATMAN, GD/X) using an acid-cleaned 20 mL all-plastic syringe. The DON samples were stored at −20 °C in acid-cleaned 20 mL scintillation vials, while the DOC samples were stored acidified with ~20 μL of ultrapure orthophosphoric acid in pre-combusted (500 °C, three hours) 4mL borosilicate vials with Teflon-lined screw caps at −20 °C until analysis in the Bangor University laboratory. The DOC and DON were analysed as described in Papadimitriou et al. (2007).

The CDOM samples were stored refrigerated in the dark in acid-cleaned plastic bottles and were measured within 24 hours of collection. The absorbance of CDOM was measured at room temperature using a dual beam Shimadzu 1601 UV-Vis spectrophotometer over the range 200 to 750 nm at a resolution of 0.5 nm. The optical density acquired from the instrument was converted to the CDOM absorption coefficient (a_{CDOM_λ}) using the equation

$$a_{CDOM_\lambda} = 2.303\frac{A(\lambda)}{r} \quad (1)$$

where $a_{CDOM\lambda}$=absorption coefficient (m^{-1}), $A(\lambda)$=optical density at a given wavelength λ, 2.303=conversion factor from $\log_{10}$ to $\log_e$ units, and r=length of optical path=0.10 m.

The CDOM absorption spectrum typically declines exponentially with wavelength (λ) when measured from 300 to 650 nm and, hence, can be modeled as an exponential function of λ (Bricaud et al., 1981). The modeled exponential slope of this spectrum (S) offers an indication of CDOM quality because it varies depending on its source (terrestrial or marine), age (fresh or old), and extent of degradation (Carder et al., 1989; Stedmon and Markager, 2001). The absorption at a specific wavelength can be used as an indicator of CDOM concentration. A range of wavelengths have been used in the past here we use 375 nm. The wavelength range from which S is calculated, and the choice of 375 nm, represents a compromise between analytical chemistry where CDOM absorption at UV wavelengths is due to its aromatic content (Chin and Gschwend, 1992), and aquatic bio-optics when predicting penetration of natural light is of interest. Reporting the absorption at 375 nm together with the S value derived from across the whole UVA and visible light range allows others to predict the light attenuation due to CDOM. The carbon-specific CDOM absorption (a^*_{375}, in $m^2\ g^{-1}$ C) is the absorption normalised to the DOC concentration (expressed in $g\ C\ m^{-3}$) and together with S represents a qualitative measure of CDOM colour.

All concentrations are reported on a per kg solution (mass) basis (C_{mass}) after conversion of the measurements on a per unit volume basis (C_{vol}) as

$$C_{mass} = \frac{C_{vol}}{\rho'} \quad (2)$$

with ρ'=sample density at the temperature of sample processing. The density of melted sea ice (ρ'_{melt}), brine (ρ'_b), and gap waters (ρ'_{gap}) in laboratory conditions were calculated by extrapolation of the equation of state for seawater in Millero and Poisson (1981) to the sample salinity, because the major ionic composition of sea ice-derived solutions reflects physical modification of that of oceanic water. The concentrations measured in melted bulk ice were further converted to per kg of brine at *in situ* temperature conditions as

$$C_{b,\ mass} = \frac{(C_{vol}/\rho'_{melt})\rho_{bulk\ ice}}{(V_b/V)\rho_b} \quad (3)$$

where (V_b/V) is the relative brine volume, and $\rho_{bulk\ ice}$ and ρ_b are the bulk ice and brine densities, respectively, at *in situ* temperature, all calculated as in Cox and Weeks (1983), using the polynomial functions in Cox and Weeks (1983) for temperatures ≤ -2 °C and Leppäranta and Manninen (1988) for temperatures between 0 > and > −2 °C and an (assumed) relative air volume of 1.5% (C. Haas, pers. comm.). The concentrations directly measured in sackhole brines and those derived from bulk sea ice measurements were

Table 1
Physical parameters measured in sea ice and brines collected during this study.

	ISPOL 27/11/04 - 02/01/05			WWOS 06/09/06 - 13/10/06		SIPEX 11/09/07 - 10/10/07	
	Bulk Ice	Brine	Surface Gap Layers	Bulk Ice	Brine	Bulk Ice	Brine
Thickness (cm)	72 to 226, n=9		1 to 16, n=23	88 to 190, n=12		35 to 133[c], n=33	
Depth (cm)		20 to 78, n=36			16 to 66[b], n=118		14 to 80, n=41
Temperature (°C)	-2.5 to -1.1[a], n=96	-3.4 to -1.3[a], n=36	-1.8 to -0.8, n=23	-8.8 to -1.9, n=154	-8.7 to - 3.6, n=126	-14.8 to -1.5, n=214	-12.4 to - 2.2, n=24
Salinity	1.0 to 9.3, n=96	29.4 to 63.2, n=40	20 to 33, n=23	0.4 to 14.1, n=154	58.1 to 134.0, n=126	2.1 to 18.3, n=251	33 to 179, n=46
V_b/V (%)	2.6 to 31.9, n=95			0.2 to 25.0, n=154		0.2 to 34.8, n=208	

[a] The brine samples were derived from the upper layers of thick first-year ice (Papadimitriou et al. 2007), which were colder than the temperature range of the ice cores obtained from spatially distinct, separate patches of thin first-year ice and thick second-year ice on the ISPOL floe.
[b] A single brine sample was obtained from a sackhole of 186 cm depth.
[c] A single 209-cm-thick ice core was obtained from rafted ice on a heavily deformed floe.

further normalised to a salinity of 35 as

$$C_{b,\,mass,s} = \frac{35}{S_b} C_{b,\,mass} \quad (4)$$

where S_b is the salinity of the brine, which, for bulk sea ice determinations, was calculated as a function of ice temperature (t, Petrich and Eicken, 2010) as

$$S_b = 1000\left(1 - \frac{54.11}{t}\right)^{-1} \quad (5)$$

The temperature and salinity of bulk ice, brine, and surface waters, as well as ice thickness and V_b/V from all three studies are given in Table 1. Correlation analysis and analysis of variance were conducted on MINITAB, while regression analysis was based on the geometric mean regression in Ricker (1973). It should be noted that not all analysis were performed on every sample mentioned in Section 2.3 above, therefore numbers of observations quoted in the following results section and accompanying tables may differ.

3. Results

3.1. Physical and biochemical parameters

3.1.1. Seawater

The mean DOC and DON concentrations in seawater varied between expeditions (Table 2), with the SIPEX samples significantly higher than both ISPOL and WWOS ($p < 0.01$) for both parameters. The concentration of POC in the water column was measured during WWOS and SIPEX and was not significantly different between cruises, while PN data were only available for SIPEX. The measured Chl*a* concentrations were all less than 0.25 μg kg^{-1} during the three studies (Table 2).

3.1.2. Bulk ice

The bulk ice temperature and salinity varied considerably between studies. The warmest ice temperatures and narrowest salinity range were encountered during the ISPOL drift experiment in the spring-summer transition (Table 1). Both the WWOS and SIPEX field studies were conducted during the winter-spring transition, yet the SIPEX data set exhibited the widest temperature and salinity ranges, including the coldest ice temperature (-14.8 °C) and highest bulk ice salinities (18.3) (Table 1).

The DOC, DON, POC, PN, and Chl*a* concentrations in the bulk ice samples exhibited a high degree of variability, with their ranges extending over 1 to 3 orders of magnitude for each parameter (Table 2). The mean DOC concentrations were not significantly different across the three studies, with at least 75% of the samples being less than 60 μmol kg^{-1} despite the large concentration ranges. The DON concentrations were lower in the SIPEX samples (significant at $p < 0.01$) than both the ISPOL and WWOS samples (Table 2). Based on all available observations from bulk sea ice, [DOC] > 200 μmol kg^{-1} and [DON] > 40 μmol kg^{-1} were measured systematically and most frequently in the bottom 10–20 cm of the cores. No other distribution pattern with depth downcore was discernible for these parameters (Fig. 2). When the measured concentrations of DOC and DON were normalised to a salinity of 35 (Gleitz et al., 1995) both constituents were enriched relative to the mean salinity-normalised concentration in the underlying seawater (Table 2). The DOC was positively correlated with DON in all studies (Fig. 3; ISPOL: $r^2_{linear} = 0.404$, $p < 0.001$, $n = 61$; WWOS: $r^2_{log-log} = 0.526$, $p < 0.001$, $n = 148$; SIPEX: $r^2_{log-log} = 0.318$, $p < 0.001$, $n = 138$). The observed DOC to DON ratios were variable within all three datasets, but the mean DOC:DON was not significantly different between them (Table 2).

The mean concentrations of POC and PN measured in the SIPEX bulk ice samples (Table 2) were lower (significant at $p < 0.001$) than those measured during ISPOL and WWOS (Table 2), with the ISPOL and WWOS mean observations being almost 3-fold and 2-fold greater, respectively (Table 2). All datasets yielded positive correlations between POC and PN (Fig. 4; ISPOL: $r^2_{log-log} = 0.297$, $p < 0.001$, $n = 57$; WWOS: $r^2_{log-log} = 0.914$, $p < 0.001$, $n = 151$; SIPEX: $r^2_{log-log} = 0.830$, $p < 0.001$, $n = 110$), with the ISPOL observations exhibiting a greater degree of scatter. Mean POC to PN ratios (Table 2) differed significantly between the studies (all $p < 0.05$).

The Chl*a* concentrations in the bulk ice samples were wide ranging in all datasets but especially in the WWOS dataset (Table 2; Fig. 5). The ranges of Chl*a* concentration in the ISPOL and SIPEX samples were similar (Table 2), but the mean for the SIPEX samples was almost half that of the ISPOL samples. The majority of the ISPOL and WWOS samples yielded Chl*a* concentrations between 1 and 7 μg kg^{-1}, whereas the majority of SIPEX samples

Table 2
Mean ± standard deviation, (range), and, number of observations (n) for measured and salinity-normalised concentrations (to a salinity of 35 and indicated by [salinity]) of dissolved constituents, and for measured concentrations of particulate constituents. All concentrations are reported in μmol kg^{-1} solution except for Chl*a*, which is reported in μg kg^{-1} solution, while the DOC:DON and POC:PN are molar ratios.

	ISPOL 27/11/04 - 02/01/05				WWOS 06/09/06 - 13/10/06			SIPEX 11/09/07 - 10/10/07		
	Seawater	Bulk Ice	Brine	Surface Gap Layers	Seawater	Bulk Ice	Brine	Seawater	Bulk Ice	Brine
DOC [measured]	47 ± 10 (29–66) n=22	47 ± 31 (20–157) n=68	216 ± 88 (23–343) n=36	87 ± 72 (19–324) n=21	37 ± 15 (14–76) n=12	44 ± 68 (6–780) n=151	300 ± 179 (114–970) n=124	53 ± 10 (38–74) n=28	42 ± 34 (7–325) n=240	160 ± 70 (17–306) n=45
DOC [salinity]	48 ± 10 (29–67) n=22	340 ± 190 (104–906) n=68	131 ± 44 (26–208) n=36	102 ± 78 (26–366) n=21	38 ± 16 (14–79) n=12	326 ± 369 (45–2420) n=151	116 ± 82 (45–475) n=124	57 ± 10 (39–78) n=28	254 ± 224 (24–1547) n=194	60 ± 31 (14–232) n=45
DON [measured]	2.5 ± 1.7 (0.5–7.8) n=66	6.1 ± 5.4 (0.5–29.9) n=85	14 ± 5 (3–26) n=38	9 ± 3 (6–15) n=20	3 ± 1 (2–6) n=19	5.1 ± 6.1 (0.2–50.2) n=150	18 ± 12 (1–84) n=126	4 ± 1 (2–6) n=28	3.7 ± 3.9 (0.2–37.0) n=242	9 ± 3 (3–16) n=46
DON [salinity]	2.6 ± 1.8 (0.5–7.8) n=66	42 ± 35 (4–156) n=85	9 ± 4 (1–20) n=38	12 ± 5 (6–23) n=20	3 ± 1 (2–6) n=19	40 ± 49 (1–267) n=150	6.8 ± 5.2 (0.2–35.4) n=126	4 ± 1 (2–6) n=28	21 ± 19 (1–159) n=200	4 ± 2 (1–11) n=46
DOC:DON	29 ± 25 (6–97) n=17	12 ± 8 (2–50) n=61	16 ± 5 (5–26) n=36	11 ± 9 (3–37) n=36	9 ± 3 (5–15) n=8	12 ± 15 (3–145) n=148	21 ± 27 (6–315) n=124	15 ± 5 (9–35) n=28	15 ± 16 (3–169) n=230	18 ± 10 (3–62) n=45
POC	3.3 ± 2.1 (0.4–5.8) n=6	128 ± 178 (6–1195) n=81	64 ± 26 (6–123) n=30	159 ± 99 (28–427) n=23	no data	78 ± 287 (3–3433) n=152	82 ± 98 (8–537) n=120	5 ± 3 (2–10) n=11	41 ± 54 (8–476) n=110	no data
PN	no data	11.6 ± 12.2 (0.2–58.9) n=58	6.0 ± 5.0 (0.9–22.8) n=25	11 ± 9 (3–41) n=23	no data	9.3 ± 37.6 (0.4–448.8) n=154	10 ± 13 (1–70) n=120	0.3 ± 0.2 (0.2–0.7) n=11	4.2 ± 8.8 (0.2–74.0) n=110	no data
POC:PN	no data	26 ± 36 (2–163) n=57	18 ± 16 (4–79) n=25	15 ± 5 (8–34) n=23	no data	10 ± 4 (5–23) n=152	9 ± 3 (5–29) n=120	15 ± 5 (10–28) n=11	19 ± 12 (3–70) n=110	no data
Chl*a*	< 0.1 n=6	7.9 ± 15.7 (< 0.1–85.4) n=95	1.1 ± 0.6 (< 0.1–2.1) n=34	7.2 ± 11.4 (0.4–44.7) n=17	all < 0.25 n=77	23 ± 185 (< 0.1–2191) n=142	2.9 ± 2.8 (< 0.1–15.1) n=91	all < 0.1 n=11	4.0 ± 10.4 (< 0.1–74.1) n=129	no data

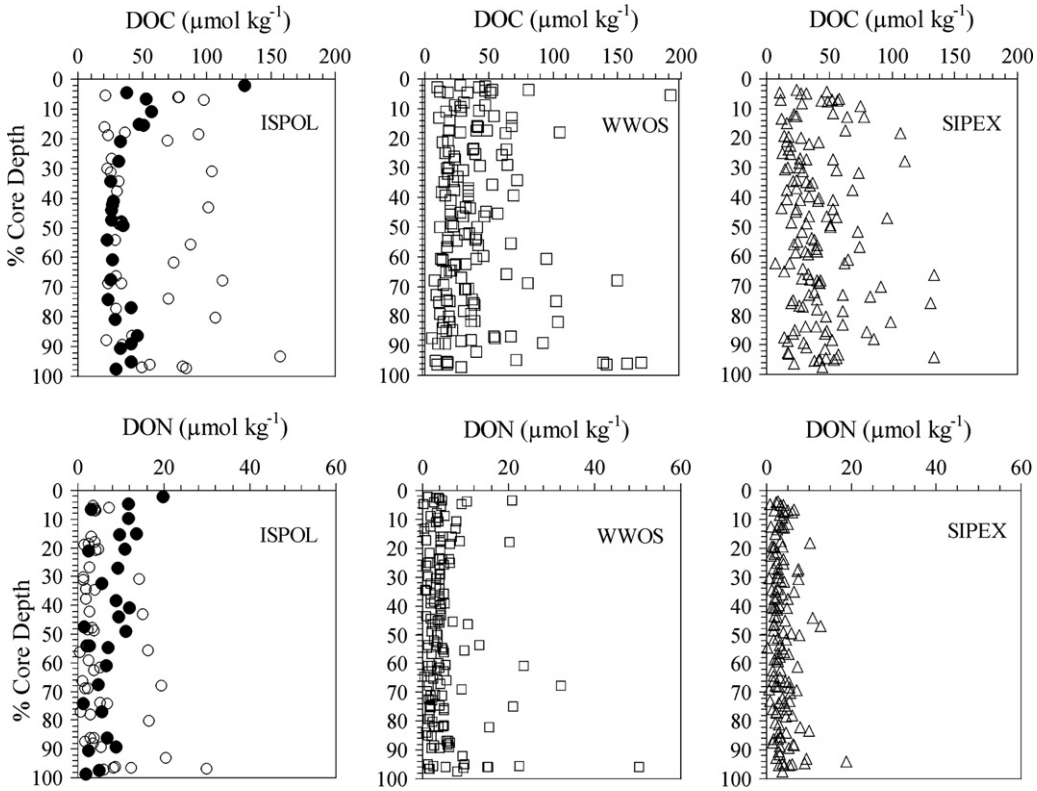

Fig. 2. Profiles of DOC and DON with depth in the ice (y=0% represents the air-ice or ice-snow interface). In the ISPOL observations, solid circles represent second-year ice with surface and internal communities, and open circles represent first-year ice. For clarity of presentation DOC concentrations > 200 µmol kg^{-1} are not included in the figures. The excluded observations were derived from the bottom section (142–155 cm depth below the ice surface) of the core obtained on 05/10/06 during WWOS ([DOC]=780 µmol kg^{-1}) and bottom section (40–43 cm depth) of the core obtained on 03/10/07 during SIPEX ([DOC]=325 µmol kg^{-1}).

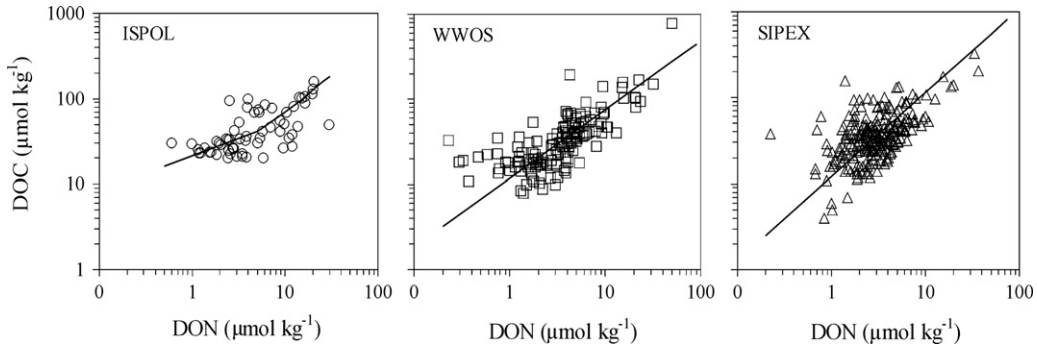

Fig. 3. DOC as a function of DON in bulk ice samples. The solid lines represent linear regressions on untransformed (ISPOL) and log-transformed data (WWOS, SIPEX). Regression equations: [DOC]=13 (±9)+6 (±1) [DON] (ISPOL), [DOC]=12 [DON] $^{0.9\ (\pm 0.1)}$ (WWOS), and [DOC]=12 [DON] $^{1.0\ (\pm 0.1)}$ (SIPEX).

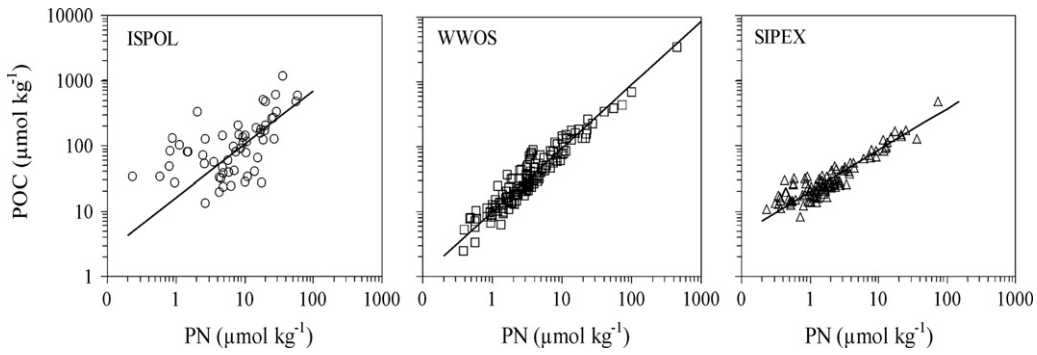

Fig. 4. POC as a function of PN in bulk ice samples. The solid lines represent regressions after log transformation of the data. Regression equations: [POC]=16 [PN] $^{0.82\ (\pm 0.19)}$, (ISPOL), [POC]=10 [PN] $^{0.98\ (\pm 0.08)}$ (WWOS), [POC]=20 [PN] $^{0.63\ (\pm 0.05)}$ (SIPEX).

yielded Chl*a* concentrations $<1\ \mu g\ kg^{-1}$. The concentrations measured in the more algal-rich parts of the ice column were also variable between expeditions, with the ISPOL samples yielding Chl*a* concentrations between 10 and 85 $\mu g\ kg^{-1}$, WWOS from 10 to 2191 $\mu g\ kg^{-1}$, and SIPEX from 3 to 46 $\mu g\ kg^{-1}$. This indicates that, at the depth of biomass maximum in sea ice, the algal biomass densities were generally most moderate during the SIPEX study and highest during the WWOS study. The depth profiles of each of the particulate constituents clearly indicated concentration maxima within the bottom 10–20 cm of the cores, except for two second-year ice cores collected during ISPOL, which exhibited localised maximum concentrations higher up in the ice column, where surface and internal communities were present (Fig. 5).

3.1.3. sea ice brine

The temperature of the sea ice brines collected during the three studies ranged between -12.4 and $-1.3\ ^{\circ}C$ and their salinities ranged from 29.4 to 179. The highest temperatures and lowest salinities were measured during ISPOL and the lowest temperatures and highest salinities were measured during SIPEX (Table 1). In sea ice, brine salinity (S_b) is reported to be a function of ice temperature (Petrich and Eicken, 2010), and this relationship was evident in the direct observations of S_b and temperature from sackhole brines during each of the studies (Fig. 6; ISPOL: $r^2=-0.956$, $p<0.001$, $n=39$; WWOS: $r^2=-0.969$, $p<0.001$, $n=124$; SIPEX: $r^2=-0.957$, $p<0.001$, $n=34$).

As with the bulk ice samples the DOC, DON, POC, PN, and Chl*a* concentrations in the brine samples exhibited a high degree of

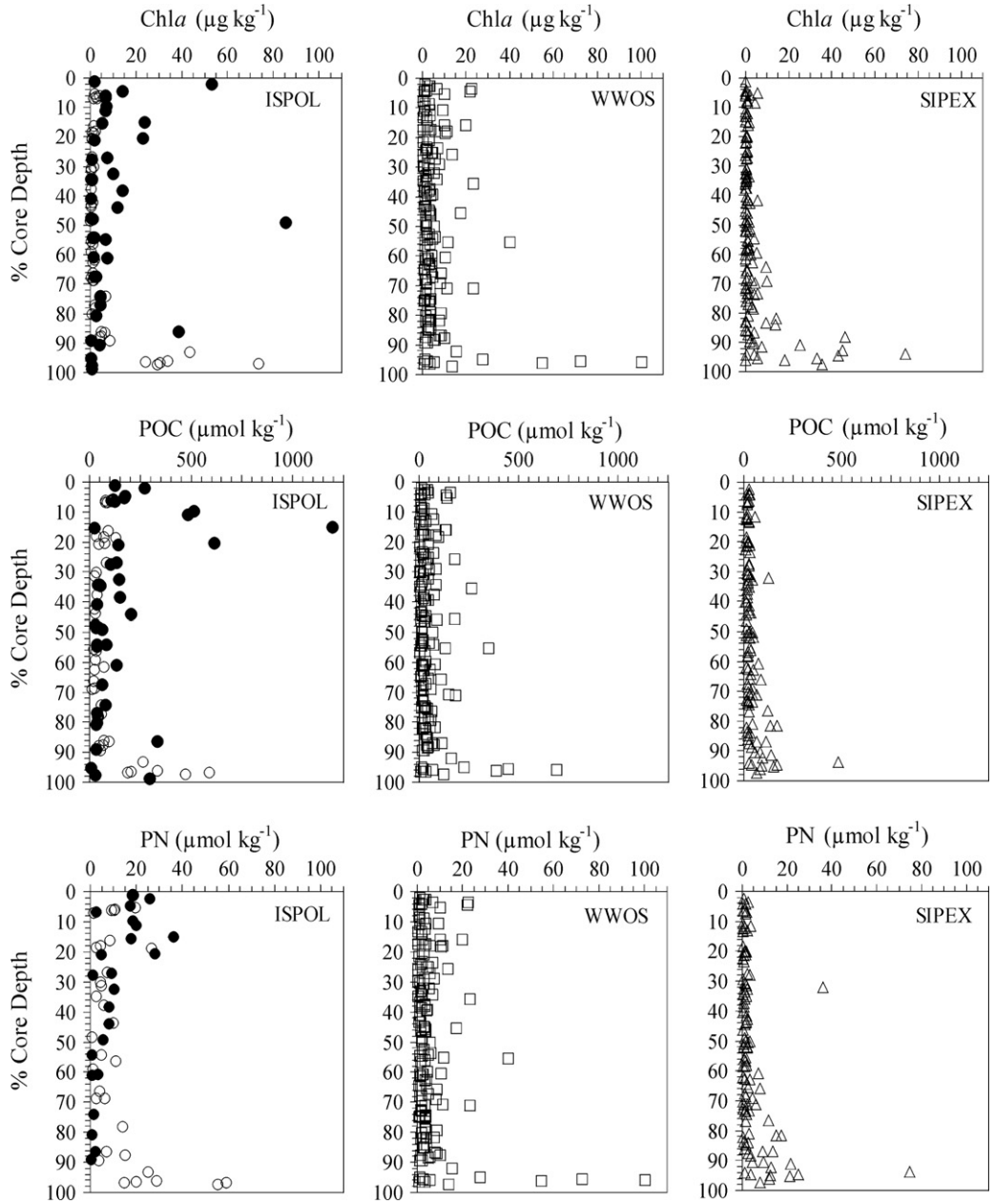

Fig. 5. Ice core profiles of POC, PN, and Chl*a*. In the ISPOL figures, solid circles represent cores from second-year ice with surface and internal communities and open circles represent cores from first-year ice. For clarity of presentation POC concentrations $>1250\ \mu mol\ kg^{-1}$, PN concentrations $>100\ \mu mol\ kg^{-1}$, and Chl*a* concentrations $>100\ \mu mol\ kg^{-1}$ are not included in the figures. The excluded observations were derived from the bottom section (142–155 cm depth below the ice surface) of the core obtained on 05/10/06 ([POC]=3433 $\mu mol\ kg^{-1}$, [PN]=449 $\mu mol\ kg^{-1}$, and [Chl*a*]=2191 $\mu g\ kg^{-1}$), and from the bottom section (111–121 cm depth) of the core obtained on 09/10/06 ([Chl*a*]=223 $\mu g\ kg^{-1}$), both during WWOS.

variability (Table 2). Mean DOC and DON concentrations were significantly different between the studies (DOC: $p < 0.005$, DON: $p < 0.03$), with the highest means and largest ranges of both parameters occurring in the WWOS brine samples (Table 2). The mean salinity-normalised concentrations of DOC and DON in sackhole brines (normalised to a salinity of 35; Gleitz et al., 1995) were higher than the salinity-normalised concentrations of the underlying seawater during ISPOL and WWOS (Table 2), indicating enrichment of DOC and DON in the sea ice brine beyond that which can be explained by simple physical concentration of these solutes. In contrast, during SIPEX, the mean salinity-normalised concentrations of DOC and DON in sackhole brines (60 ± 31 μmol kg^{-1} and 3.9 ± 1.8 μmol kg^{-1}, respectively) were similar to the mean salinity-normalised seawater concentrations (57 ± 10 and 3.9 ± 1.0 μmol kg^{-1}, respectively). The DOC and DON measurements in the brines were positively correlated, (Fig. 7; ISPOL: $r^2 = 0.808$, $p < 0.001$, $n = 31$; WWOS: $r^2 = 0.772$, $p < 0.001$, $n = 122$; SIPEX: $r^2 = 0.438$, $p = 0.031$, $n = 29$), and although the observed DOC:DON was variable within all three datasets, the mean DOC:DON did not differ significantly between the datasets (Table 2). Within the ISPOL and SIPEX datasets, there was a small proportion of observations ($< 10\%$) that had a lower DOC:DON (≤ 10) than the majority of samples (range = 14 to 30; Table 2). These observations were excluded from the regression analysis shown in Fig. 7.

The POC and PN concentrations were all elevated in the WWOS brine samples compared to the ISPOL samples (Table 2), but they were not significantly different. The measured concentrations of both parameters were highly variable during both campaigns, although there appeared to be some degree of consistency within locations, particularly during the WWOS field study. The POC and PN of the brines were positively correlated (Fig. 8; ISPOL: $r^2_{linear} = 0.163$, $p = 0.032$, $n = 23$; WWOS: $r^2_{log-log} = 0.907$, $p < 0.001$, $n = 120$). The two highest PN observations (19.2 and 22.9 μmol kg^{-1}) from the ISPOL data set were excluded as the concentrations were 3- to 4-fold higher than any other sample measured and disproportionally influenced the analysis. As with the bulk ice samples, the mean POC:PN differed between the two studies at 18 ± 16 (ISPOL) and 9 ± 3 (WWOS), which may be attributed to the difficulties encountered when sampling particulate matter from sackhole brines.

The Chl*a* concentrations in WWOS brine samples were higher than the ISPOL brine samples (significant at $p < 0.001$), with the majority of the WWOS brine samples yielding Chl*a* concentrations between 2 and 5 μg kg^{-1} and all ISPOL samples yielding < 2.1 μg kg^{-1}. No Chl*a* data are available from the SIPEX brine samples. As with the POC and PN, the reported Chl*a* concentrations in the brine are only an approximation of the *in situ* concentrations.

3.1.4. Surface gap layers

The biogeochemical composition of the two surface gap layers sampled during the ISPOL study has been reported in Papadimitriou et al. (2009). Briefly, the concentrations of the biogenic dissolved and particulate matter were within the ranges observed in bulk sea ice, with higher DOC, DON, POC, PN, and Chl*a* concentrations in the waters of the thick gap layer overlying second-year ice than those in the water of the thin gap layer overlying thick first-year ice. Additional biogeochemical measurements (pH, dissolved molecular oxygen, major dissolved inorganic nutrients, including total dissolved inorganic carbon), however, indicated comparable autotrophic activity in both gap layers by the surface biological assemblage which extended in the neighboring surface ice layers. Mean values, standard deviations, and ranges are given in Table 2.

3.2. CDOM

The absorption spectra of seawater followed the commonly observed exponential decline with increasing wavelength (Bricaud et al., 1981), but the bulk ice, brine, and gap water samples did not. Many of the bulk ice and brine samples, and all of the gap water samples had a distinct peak at 320–330 nm, with the bulk ice samples also displaying a shoulder between 260 and 280 nm. These features were consistent across all three studies (Figs. 9 and 10). Using 375 nm (a_{375}) as an indicator of CDOM concentration, all studies yielded the highest concentrations in the brine samples, with mean values 4 times greater than in the underlying seawater (Table 3). No significant differences were found in a_{375} between the studies. The carbon-specific CDOM absorption (a^*_{375}) was highest in the bulk ice samples, with a maximum value of 2.38 m^2 g^{-1} C (Table 3).

Due to the presence of the shoulders and peaks, none of the gap water spectra, only 12% of the ice spectra, and 47% of the brine spectra could be modeled with an exponential function.

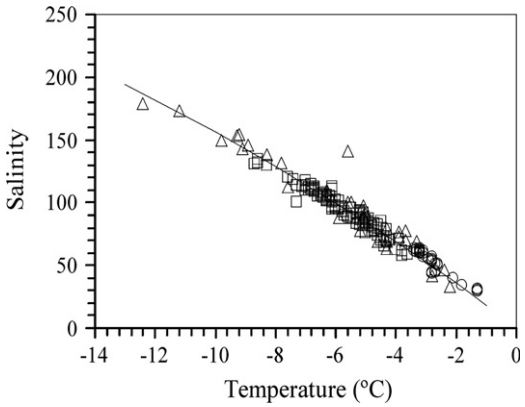

Fig. 6. Salinity as a function of temperature in sea ice brines. The open circles represent ISPOL samples, open squares represent WWOS samples, and open triangles represent SIPEX samples. The solid line represents the functional relationship between the two parameters as described by Petrich and Eicken (2010).

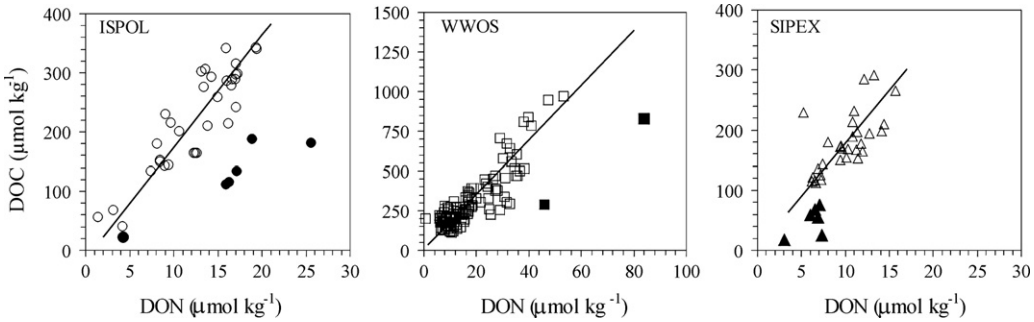

Fig. 7. DOC as a function of DON in sea ice brines. The solid lines represent linear regressions. The solid symbols in all graphs represent observations not included in the regression analysis. Note that the WWOS data is presented on a different scale from the ISPOL and SIPEX data due to the much larger concentration range measured. Regression equations: [DOC] = −17 (±42)+19 (±3) [DON] (ISPOL), [DOC] = 15 (±28)+17 (±1) [DON] (WWOS), [DOC] = 1 (±52)+18 (±5) [DON] (SIPEX).

The S values obtained from this sub-set of the data show very similar means and ranges in the seawater and brine samples, whereas the bulk ice samples exhibited a lower mean and minimum value than that of the seawater and brine samples (Table 3). In contrast the a^*_{375} of the bulk ice samples was more than double that of the brine and almost double that of the seawater (Table 3). When S was plotted against the a^*_{375} of the brine and seawater samples, all observations followed the same trend, with higher S values and low a^*_{375} in seawater and brine and low S and high a^*_{375} in bulk sea ice (Fig. 11).

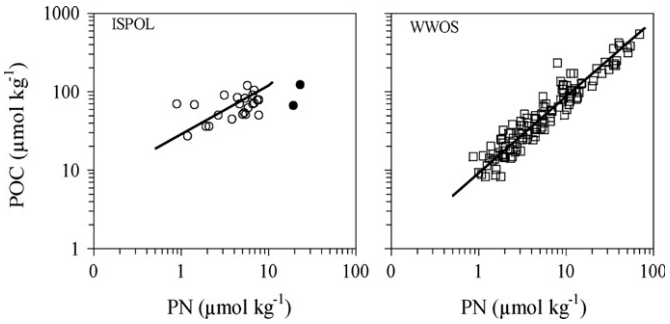

Fig. 8. POC as a function of PN in sea ice brine. The solid lines represent regressions on measured (ISPOL) and log transformed concentrations (WWOS). Solid circles on the ISPOL graph represent observations not included in the regression analysis. Regression equations: [POC]=14 (±21)+11 (±4) [PN] (ISPOL), [POC]=9 [PN] $^{0.97\ (\pm 0.08)}$ (WWOS).

3.2.1. Relationships with physical and biogeochemical parameters.

In order to investigate possible relationships between the biogeochemical and physical parameters (DOC, DON, POC, PN, Chl*a*, temperature, and salinity) and the optical measurements (CDOM), the absorption spectra of each sample type (seawater, bulk ice, brine, and surface gap layer) were divided into four wavelength bands, and the integrated CDOM absorption coefficient ($a_{CDOM\lambda}$) within those bands was calculated for each sample. Bands 1 (250 to 255 nm) and 4 (390 to 400 nm) represented the background CDOM, band 2 (265 to 270 nm) contained the highest point of the shoulder observed in the bulk ice samples, and band 3 (320 to 330 nm) contained the top of the peak observed in the bulk ice, brine, and gap water samples (see Fig. 9). Between studies the $a_{CDOM\lambda}$ at band 3 in the WWOS bulk ice samples was lower than in both the ISPOL and SIPEX samples (significant at $p=0.001$ and $p<0.001$, respectively), and in the brine samples the $a_{CDOM\lambda}$ of the SIPEX brine samples was lower than in both ISPOL and WWOS brine samples at all bands (significant at $p<0.05$) (Table 4). No additional information was gained as to the source of the peaks from the correlation analysis of the wavelength bands with the physical and biochemical parameters.

3.3. Photo-bleaching experiment

3.3.1. Light measurements

The maximum UVR values reached 4.70 W m^{-2} at $t=1$ h, and 70.31 W m^{-2} at $t=72$ h (between 1500 and 1600 ship time (UTC -4)) for the UVB and UVA bands, respectively, while the minimum values reached 0.02 W m^{-2}, initially at $t=12$ h and then at each

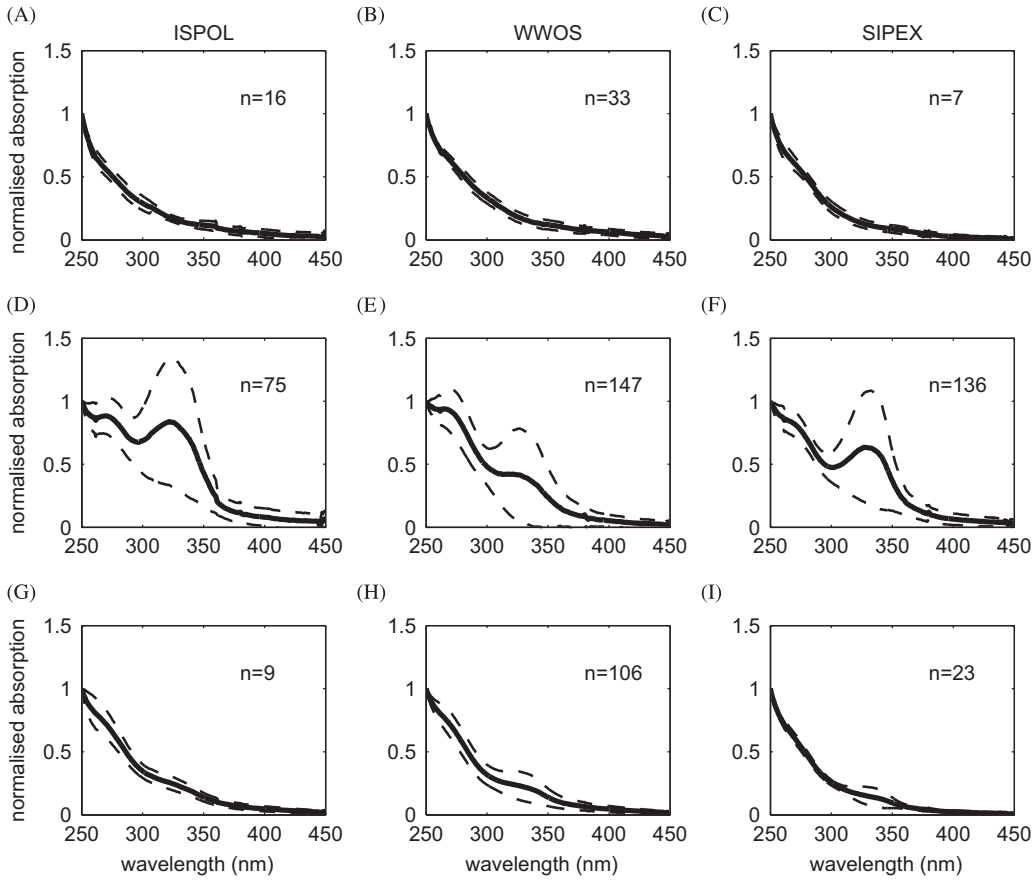

Fig. 9. Seawater, bulk-ice, and brine absorption spectra. Data presented are means and standard deviations of normalised absorption spectra (value at 250 nm normalised to 1). (A), (B), (C)=seawater samples, (D), (E), (F)=ice core section samples, (G), (H), (I)=brine samples.

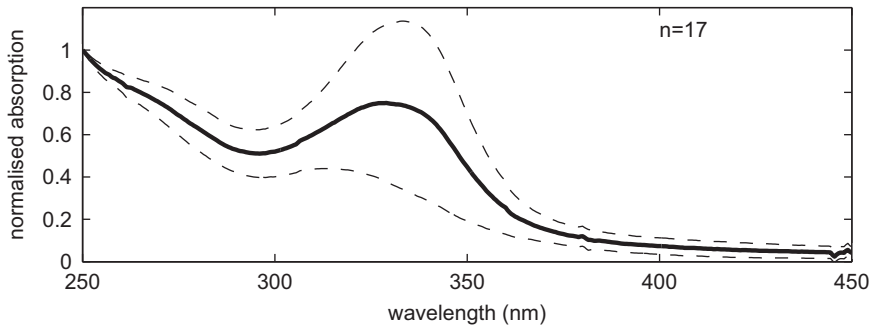

Fig. 10. Absorption spectra from water samples collected from two gap layers during the ISPOL drift experiment in the Weddell Sea between 27/11/04–02/01/05. Data presented are means and standard deviations of normalised absorbance spectra (value at 250 nm normalised to 1).

Table 3
Mean ± standard deviation, (range), and number of observations (n) for the samples from Antarctic sea ice and surface oceanic waters from which optical measurements of DOM (CDOM) were obtained: CDOM absorption coefficient ($a_{CDOM\lambda}$) at 375 nm (a_{375}) and average between 320 and 330 nm ($\hat{a}_{320\text{-}330}$, corresponding to the peak observed in Figs. 9 and 10), spectral slope (S calculated from the exponential model fit on individual 300–650 nm spectra), carbon-specific absorption (a^*_{375}), and corresponding dissolved organic carbon (DOC) concentrations. For many samples from the brines and ice cores, and for all of the surface gap layer samples it was not possible to model the absorption spectra using an exponential model (see Figs. 9 and 10 for indication of these non-exponential spectral shapes) and *S* could therefore not be calculated.

	Seawater	Ice	Brine	Surface Gap Layer
a_{375} (m^{-1})	0.11 ± 0.11 (0.01-0.78) n=54	0.14 ± 0.16 (0.00-1.43) n=358	0.41 ± 0.37 (0.00-1.79) n=138	0.28 ± 0.14 (0.07-0.68) n=23
$\hat{a}_{320\text{-}330}$ (m^{-1})	0.29 ± 0.55 (0.06-4.23) n=54	0.56 ± 0.46 (0.03-2.83) n=358	1.23 ± 0.99 (0.12-4.52) n=138	1.34 ± 0.77 (0.34-3.37) n=23
S (μm^{-1})	20.9 ± 6.1 (11.1-39.6) n=51	16.2 ± 6.9 (6.5-33.3) n=42	20.2 ± 4.1 (13.7-34.6) n=65	No Data
a^*_{375} ($m^2\ g^{-1}$ C)	0.19 ± 0.18 (0.04-0.94) n=27	0.33 ± 0.37 (0.00-2.38) n=320	0.13 ± 0.09 (0.00-0.46) n=130	0.56 ± 0.47 (0.08-1.71) n=18
DOC ($\mu mol\ kg^{-1}$)	47 ± 14 (14-76) n=43	42 ± 30 (6-192) n=320	271 ± 172 (23-970) n=137	84 ± 75 (18-324) n=20

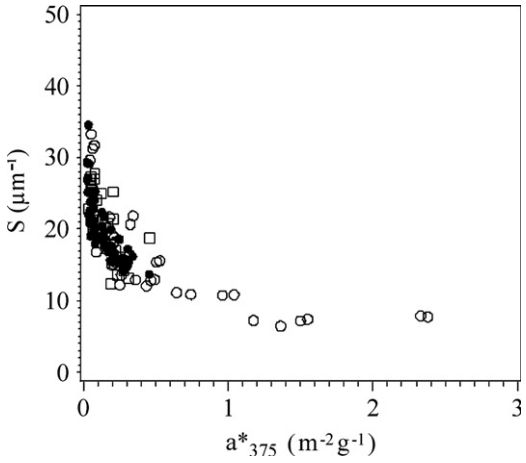

Fig. 11. Spectral slope (S, 300-650 nm) as a function of the carbon-specific absorption coefficient (a^*_{375}). Solid circles represent brine, open circles represent bulk ice, and open squares represent seawater.

24 h interval thereafter, and 0.81 W m^{-2} at $t=12$ h (between 03:00 and 04:00 ship time), respectively (Fig. 12; daily averages given in Table 5). Due to methodological restraints imposed by the type of sensor used, the PAR data could only be expressed in µmol m^{-2} s^{-1}. Here the maximum values were around 2500 µmol m^{-2} s^{-1} at $t=72$ h (local noon), while minimum values reached ~20 µmol m^{-2} s^{-1} at local midnight (Fig. 12).

3.3.2. Biogeochemical parameters

The shoulders and peaks observed in many of the brine samples were not present in the brine collected for the photo-bleaching experiment. Therefore, in addition to 375 nm it was possible to add two further reference wavelengths of 280 nm and 330 nm to calculate a percentage change in CDOM absorbance over the 120 h experimental period. A clear decrease in $a_{CDOM\lambda}$ was observed at 280 and 330 nm in the light-exposed brine samples, with little change observed in the dark control samples (Fig. 13). The 120 h exposure to photo-bleaching resulted in a 53% decrease in $a_{CDOM\lambda}$ at 280 nm and 58% decrease at 330 nm (Table 6; Fig. 14). In contrast, $a_{CDOM\lambda}$ at 375 nm initially increased by 12% in the light-exposed samples during the first 24 h of the experiment. An overall decrease in $a_{CDOM\lambda}$ of 30% from the initial concentration was measured at $t=48$ h, and no further change was observed at $t=120$ h (Table 6; Fig. 14). The control samples increased throughout the experiment and a 48% increase in $a_{CDOM\lambda}$ at 375 nm was measured at $t=120$ h (Table 6; Fig. 14). Some variability in DOC

Table 4
Mean ± standard deviation and (range) for integrated CDOM absorbance coefficients ($a_{CDOM\lambda}$) within wavelength bands 250 to 255 nm (band 1), 265 to 270 nm (band 2), 320 to 330 nm (band 3) and 390 to 400 nm (band 4) in seawater, bulk ice, brine and gap layer samples Bands 1 and 4 represent background CDOM, while bands 2 and 3 represent the location of spectral peaks.

	ISPOL 27/11/04 - 02/01/05				WWOS 06/09/06 - 13/10/06			SIPEX 11/09/07 - 10/10/07		
	Seawater, n=10	Bulk Ice, n=74	Brine, n=8	Gap layers, n=20	Seawater, n=32	Bulk Ice, n=142	Brine, n=105	Seawater, n=7	Bulk Ice, n=134	Brine, n=18
Band 1 250 to 255 nm	0.97 ± 0.18 (0.66-1.18)	0.82 ± 0.77 (0.13-6.3)	4.3 ± 2.1 (1.1-6.2)	1.8 ± 0.50 (0.95-2.92)	0.96 ± 0.14 (0.71-1.26)	1.0 ± 1.5 (0.22-16.5)	5.5 ± 3.6 (2.1-21.1)	1.6 ± 0.75 (0.98-3.2)	0.95 ± 0.51 (0.34-3.8)	2.8 ± 1.2 (0.97-5.5)
Band 2 265 to 270 nm	0.65 ± 0.14 (0.42-0.79)	0.79 ± 0.96 (0.11-8.1)	3.5 ± 1.8 (0.8-5.2)	1.5 ± 0.54 (0.70-2.8)	0.69 ± 0.12 (0.45-0.96)	1.1 ± 1.7 (0.17-19.2)	4.6 ± 3.5 (1.4-20.2)	1.2 ± 0.54 (0.68-2.3)	0.82 ± 0.45 (0.27-3.7)	1.9 ± 0.84 (0.71-3.9)
Band 3 320 to 330 nm	0.18 ± 0.04 (0.14-0.26)	0.59 ± 0.41 (0.07-1.7)	1.1 ± 0.47 (0.33-1.6)	1.5 ± 0.68 (0.43-3.2)	0.20 ± 0.06 (0.06-0.33)	0.39 ± 0.42 (0.03-2.7)	1.4 ± 1.0 (0.16-4.5)	0.25 ± 0.12 (0.12-0.47)	0.62 ± 0.48 (0.09-2.7)	0.48 ± 0.27 (0.12-1.1)
Band 4 390 to 400 nm	0.06 ± 0.03 (0.03-0.12)	0.06 ± 0.05 (0.00-0.21)	0.23 ± 0.13 (0.03-0.33)	0.14 ± 0.07 (0.06-0.40)	0.07 ± 0.03 (0.01-0.15)	0.07 ± 0.09 (0.00-0.73)	0.32 ± 0.28 (0.00-1.2)	0.05 ± 0.04 (0.01-0.09)	0.07 ± 0.08 (0.00-0.44)	0.08 ± 0.05 (0.00-0.2)

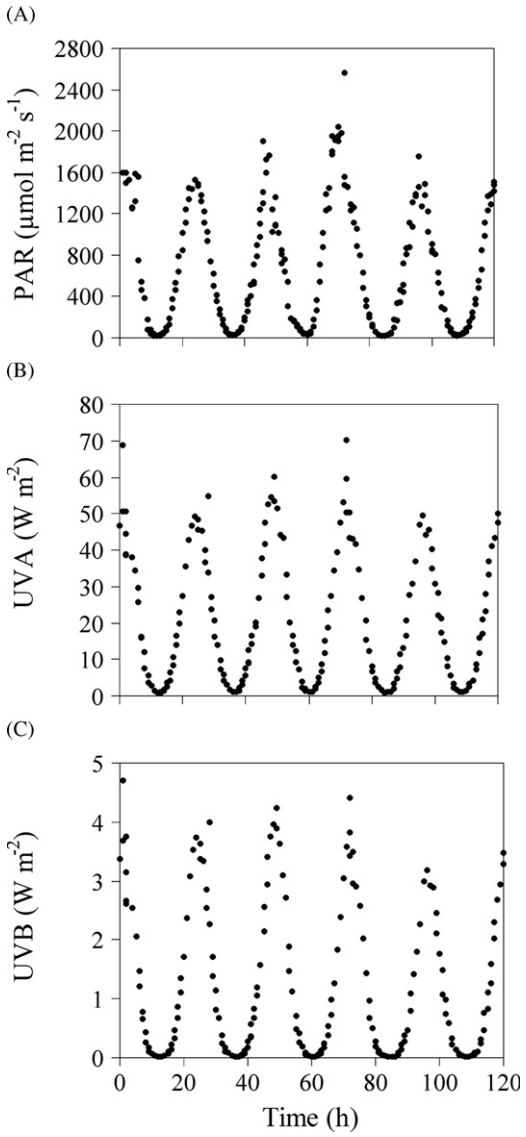

Fig. 12. PAR (A), UVA (B) and UVB (C) measurements during a CDOM photo-bleaching experiment on the ISPOL ice floe between 1500 (t=0 h) 06/12/04 and 1500 (t=120 h) 10/12/04. PAR data are expressed in µmol m^{-2} s^{-1}, and UVR data are expressed in W m^{-2}. Note difference in scale of Y axis.

Table 5
UVA and UVB daily doses (kJ d^{-1}) during CDOM photo-bleaching experiment on the ISPOL floe. The calculations are based on hourly averages.

Day	UVA (kJ d^{-1})	UVB (kJ d^{-1})
06/12/04	1793.61	114.89
07/12/04	1646.07	117.91
08/12/04	2138.84	127.20
09/12/04	1730.77	99.14
10/12/04	1739.00	99.05

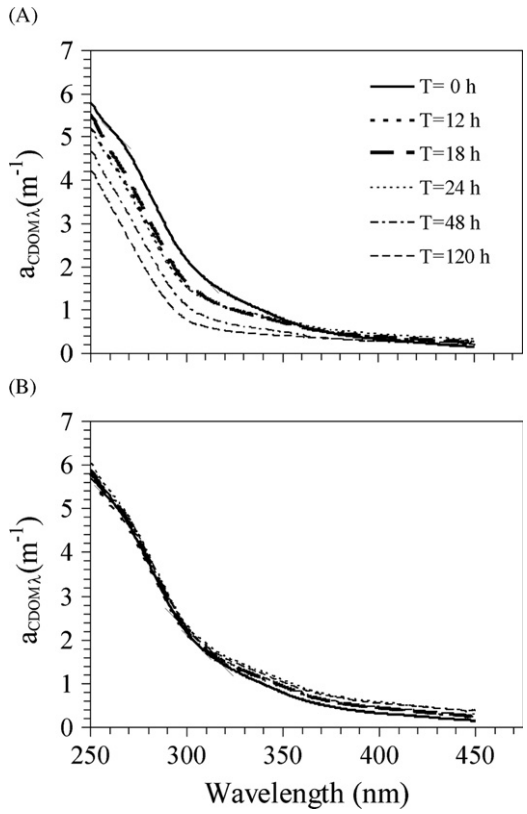

Fig. 13. Changes in CDOM absorbance spectra over time (t=0 to t=120 h) in sea ice brine exposed to light (A) and dark control (B) *in situ* during a CDOM photo-bleaching experiment set up during ISPOL in order to investigate the bleaching dynamics of brine CDOM. Brine salinity=55.2.

Table 6
Spectral slope (S, calculated from the exponential model fit on individual 300–650 nm spectra), CDOM absorption coefficient ($a_{CDOM\lambda}$) at 280 nm (a_{280}), 330 nm (a_{330}), and 375 nm (a_{375}), carbon-specific absorption (a^*_{375}), and corresponding DOC and DON concentrations (μmol kg^{-1}) during the CDOM photo-bleaching experiment on the ISPOL floe (brine salinity=55.2).

Treatment	Time Point (hr)	S (μm^{-1})	a_{280} (m^{-1})	a_{330} (m^{-1})	a_{375} (m^{-1})	a^*_{375} ($m^2\ g^{-1}$ C)	DOC (μmol kg^{-1})	DON (μmol kg^{-1})
Initial Value	0	23.10	3.8	1.2	0.47	0.16	249	18.4
Light Exposed	12	27.78	3.1	0.9	0.48	0.16	251	12.6
	18	28.03	2.9	0.9	0.48	0.16	254	16.2
	24	28.68	2.9	1.0	0.54	0.18	251	12.3
	48	33.82	2.4	0.6	0.33	0.11	257	15.0
	120	35.62	1.8	0.5	0.33	0.11	249	15.2
Dark Control	12	23.31	3.9	1.3	0.58	0.19	252	13.5
	18	23.07	3.9	1.4	0.59	0.19	251	15.9
	24	22.81	3.9	1.3	0.72	0.23	261	14.7
	48	23.12	3.8	1.3	0.70	0.19	261	18.1
	120	23.26	3.7	1.3	0.70	0.24	247	13.9

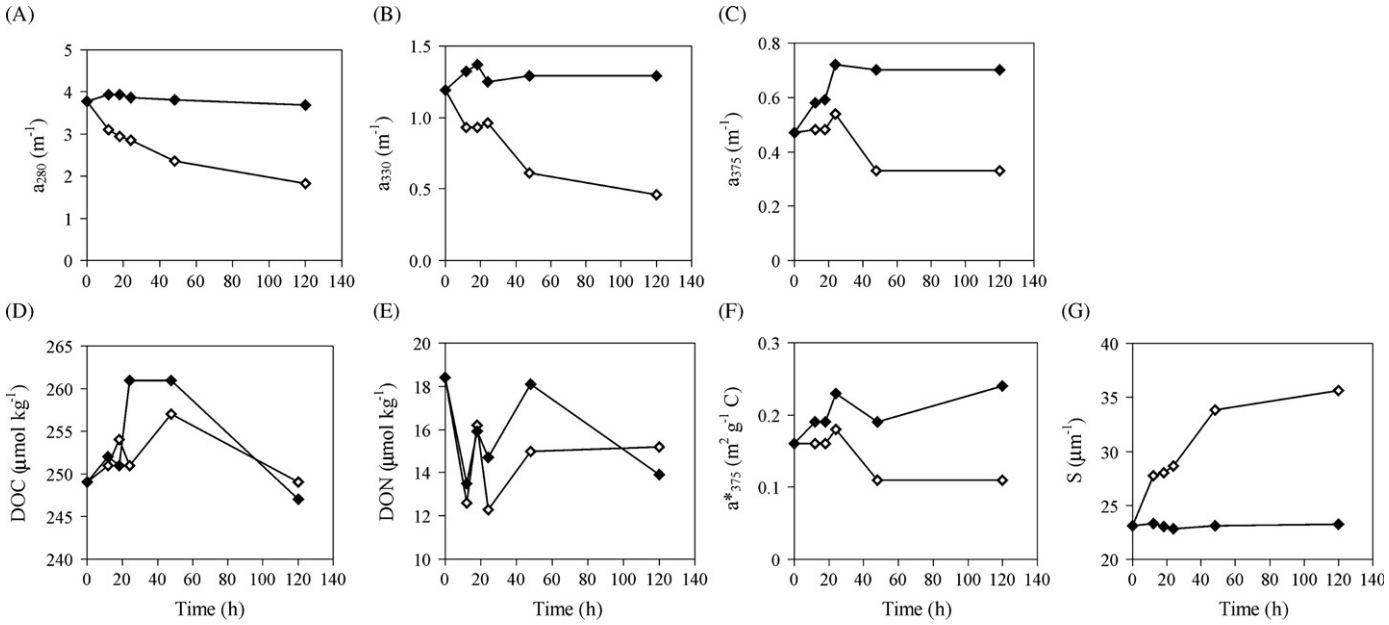

Fig. 14. Changes in $a_{CDOM\lambda}$ at 280 nm (a_{280}) (A), 330 nm (a_{330}) (B), 375 nm (a_{375}), (C), DOC (D) and DON (E) concentrations (μmol kg^{-1}), carbon-specific absorption (a^*_{375}) (F), and spectral slope (G) (S, calculated from the exponential model fit on individual 300–650 nm spectra), over time for a CDOM photo-bleaching experiment set up during ISPOL in order to investigate the bleaching dynamics of brine CDOM. Brine salinity=55.2. Open symbols represent light exposed samples, and filled symbols represent dark (control) samples.

from the initial concentration of 249 μmol kg^{-1} was observed in both sample sets, with increases of 3.2% in the light exposed samples, and a 4.8% in the control samples occurring in the first 48 h of the experiment. However, DOC in both sample sets returned to the initial concentration (Light: 249 μmol kg^{-1}; Control: 247 μmol kg^{-1}) by the end of the experiment (Table 6, Fig. 14). A loss of DON from the starting concentration of 18.4 μmol kg^{-1} was evident in both treatments (Light at t=120 h: 15.2 μmol kg^{-1}; Control at t=120 h: 13.9 μmol kg^{-1}) (Table 6; Fig. 14).

The overall trend of the a^*_{375} in the light-exposed samples was a decline from 0.16 $m^2\ g^{-1}$ C at t=0 to 0.11 $m^2\ g^{-1}$ C at t=120 h, save for a small rise at t=24 h to 18 $m^2\ g^{-1}$ C. In the dark (control) samples, the overall trend was an increase in a^*_{375} to 0.24 m^{-1}, suggesting production of light-absorbing carbon-specific CDOM in the control samples during the experimental period (Table 6; Fig. 14). However, the observed variability in DOC concentration was not coincident with the variability of the a^*_{375} in either sample set.

The S value at t=0 was 23.1 μm^{-1}, with the dark (control) samples varying little from this value throughout the duration (120 h) of the experiment (range: 22.8 to 23.3 μm^{-1}). In contrast, the light- exposed samples exhibited a steady and significant increase in S (p=0.006), with a final value of 35.6 μm^{-1} at t=120 h (Table 6; Figs. 13 and 14).

4. Discussion

4.1. Biogeochemical parameters

The sources of organic matter (i.e. incorporation from the underlying seawater and *in situ* production) are likely to be broadly the same for each of the studies reported here. It is reasonable to expect that although the quantity of material will be variable depending on seasonal ice growth and decay (e.g., younger ice encountered during SIPEX generally had lower concentrations of the measured parameters than the ISPOL and WWOS ice), the quality of the material will not vary between the studies.

The DOC and POC concentrations in seawater measured during ISPOL and WWOS are within the range previously measured in the Weddell Sea during summer and winter, respectively (Garrison and Close, 1993; Wedborg et al., 1998; Herborg et al., 2001; Ogawa and Tanoue, 2003; Dumont et al., 2009; Ortega-Retuerta et al., 2010).

The SIPEX seawater DOC and POC concentrations are comparable with previously reported concentrations for the same time of year, and from the same area in the Southern Ocean (Dumont et al., 2009). The elevated mean DOC and DON concentrations of the SIPEX samples compared to the ISPOL and WWOS samples may be attributed to the sampling strategy, where full under-ice seawater depth profiles were measured during ISPOL and WWOS, whereas all SIPEX seawater samples were collected at between 1 and 10 m depth. In all three studies, save for a small number of cores exhibiting internal and surface biomass maxima, the highest concentrations of all measured biogeochemical parameters were found in the bottom 10 to 20 cm of the ice column. The WWOS maximum values were all elevated in comparison to ISPOL and SIPEX, indicating that there was considerably more biomass present in the bottom sections of the ice during the WWOS study than during the other two studies.

The mean salinity-normalised bulk ice DOC and DON concentrations were, in all studies, enriched relative to the salinity-normalised concentrations of the underlying seawater, which suggests further *in situ* production to that incorporated from the surface ocean as the ice formed. Thomas et al. (2001), Herborg et al. (2001), and Kattner et al. (2004) report mean bulk ice DOC concentrations of 109 μM, 207 μM, and 254 μM in summer sea ice from the Weddell Sea, which are 2- to 5-fold greater than the mean values reported here. Mean brine DOC concentrations reported in Thomas et al. (2001) are also 2- to 4-fold higher than the concentrations reported in this study.

The range of DOC concentrations in the bulk ice reported from the ISPOL study by Dumont et al. (2009) were 106 to 701 μM C as opposed to the much lower range reported here of 20 to 157 μM. The two sets of samples were taken from different areas on the floe, and this variability is an example of the heterogeneity of a single ice floe (Eicken et al., 1991). Similarly, the bulk ice DOC ranges reported here for the SIPEX study and in Dumont et al. (2009) for the ARISE study (2003) were quite different, despite the similar ice conditions (Lannuzel et al., 2007) of the two studies, with the SIPEX mean DOC concentration being half that of the lowest reported measurement from the ARISE ice samples.

All three studies exhibited a large range of DOC to DON ratios in the bulk ice samples, reflected in the relatively low but still significant correlations, with DOC:DON >50 observed in all studies and DOC:DON >140 observed in both WWOS and SIPEX studies. All but one of the samples associated with these high DOC:DON values had a DOC concentration that was close to the mean DOC concentrations. This indicates that these high ratios were due to N depletion rather than C enrichment, although no evidence could be found to indicate that DON had been incorporated into the POM. The mean DOC:DON ratios of all three studies were similar to the mean value of 11 reported by Thomas et al. (2001) from samples collected in the southeastern Weddell, Bellingshausen, and Amundsen seas in summer.

The mean concentration and upper concentration range of the POC, PN, and Chl*a* measured in the bulk ice during SIPEX were all much lower than those measured in the ISPOL and WWOS studies. All the measured biogeochemical parameters from the SIPEX bulk-ice and brine samples had lower concentrations than those of ISPOL and WWOS. The mean POC concentrations measured in the SIPEX samples were also half of that reported in young Weddell Sea winter ice by Garrison and Close (1993), whereas the POC concentrations reported for the ISPOL samples were similar to summer low to medium biomass values reported by Kattner et al. (2004). In addition, the majority of cores the collected during SIPEX were <100 cm with half of these being <55 cm thick, whereas the cores collected during ISPOL and WWOS were >70 cm thick, with most being ≥ 100 cm thick. The lower biomass and thinner ice during SIPEX indicates an environment of young winter ice growth with low biomass compared to the older first- and second-year ice from ISPOL and WWOS.

The mean bulk ice POC:PN values reported here in the WWOS samples were similar to the value of 9.5 ± 5.6 reported by Kennedy et al. (2002), with the SIPEX samples being slightly elevated by comparison. In contrast the POC:PN values of the ISPOL samples (mean: 26 ± 36; Table 2) were considerably higher. These elevated POC:PN values appear to be a reflection of a mostly non-living as opposed to actively growing community (Kattner et al., 2004), as may be expected in spring/summer ice.

4.2. CDOM absorption and optical properties

The seawater CDOM concentrations (a_{375}) were within the range expected for oceanic waters (Blough and Del Vecchio, 2002), but mean a_{375} in the melted ice cores was lower than the values reported in young Arctic sea ice (Belzile et al., 2000). For the CDOM spectra that could be modeled with an exponential relationship, the resulting S values followed the trend expected from mixing of fresh and old marine CDOM (Stedmon and Markager, 2001), with fresh CDOM having low S values ($\sim 10\ \mu m^{-1}$) and the old marine CDOM having very low concentrations ($a_{375} < 0.05\ m^{-1}$) and higher S values ($S \sim 20$ to $30\ \mu m^{-1}$). The carbon-specific CDOM absorption was highest in the melted ice cores, with a maximum value of $2.4\ m^2\ g^{-1}$ C. These values are similar to those reported for terrestrial material in the Baltic region and Arctic rivers (Stedmon et al., 2000), which indicates that CDOM production in the ice generates material which is as intense in colour as terrestrial material. For comparison, the seasonal production of CDOM in the surface waters of the North Atlantic generated CDOM with an $a^*_{375} < 0.3\ m^2\ g^{-1}$ C. Plotting the S values versus the carbon specific absorption values reveals the characteristics of CDOM for the two general end-members present (Fig. 11). This indicates that the optical characteristics of the CDOM pool across all samples and locations in the current study can be broadly described by the mixing of two end-members; with fresh material, characterised by low S values and more chromophores (i.e. high a^*_{375}) as one end-member, and older material, typically characterised by high S and low a^*_{375}, as the other. S values have been found to be inversely proportional to the average molecular weight of DOM, with high molecular weight material having low S values and low molecular weight material high S values (Blough and Green, 1995). This indicates that the fresh material referred to above has a high molecular weight DOM. This would be in agreement with the size-reactivity continuum model of Amon and Benner (1996) whose results indicated that the origins of high molecular weight components are generally more recent than those of low molecular weight components. Moreover, the results presented here are also in agreement with those of Belzile and Guo (2006) who showed that low DOC-specific DOM was less coloured and of a lower molecular weight than high DOC-specific DOM.

Peaks in CDOM absorbance spectra similar to those observed here (Figs. 9 and 10) have been identified in both natural and experimental samples. Belzile et al. (2000) reported peaks of this type in ice core samples from the Northern Baffin Bay. Patsayeva et al. (2004) also observed peaks between 270 and 300 nm in brine samples generated in an ice tank experiment, and Ortega-Retuerta et al. (2010) observed peaks below 300 nm in Southern Ocean seawater used in CDOM photochemical experiments, particularly in those where Chl*a* and bacterial abundance were high. Similar absorbance spectra have also been found to be present in the CDOM produced by cyanobacteria in culture (Steinberg et al., 2004). The shoulders observed in this study between 260 to 280 nm (constrained in band 2 at 265 to 270 nm) are likely to be associated with aromatic amino acids, such as tryptophan and tyrosine, which

exhibit a strong absorbance band at ~280 nm, and can contribute significantly to the absorption of UV radiation (Wozniak and Dera, 2007). A number of mycosporine-like amino acids (MAAs), which are UV-absorbing compounds, have been identified with absorbance maxima in the 310 to 360 nm spectral range (Nakamura et al., 1982; Karentz et al., 1991; Shick et al., 1992; Davidson et al., 1994). Riegger and Robinson (1997) observed absorption maxima in the 330 to 333 nm range in 9 out of 11 cultured Antarctic diatom species, which, they suggested, indicated the presence of UV-absorbing compounds, such as MAAs, while Fritsen et al. (2011) have also suggested MAAs as a likely contributor to particulate absorption peaks at ~325 nm observed in ice samples from the Bellingshausen Sea. The peaks between 320 and 330 nm measured in this study may therefore be associated with MAAs, as they were markedly high also in samples from the two surface gap layers (Fig. 10), which represents an environment exposed to high solar radiation. MAAs (especially shinorine and palythine) have indeed been shown to contribute significantly to UV absorption in thin snow free sea ice in the Baltic Sea (Uusikivi et al., 2010), with absorption peaks in the 320 to 330 nm range for particulate matter in surface ice layers, indicative of significant production of MAAs by ice algae. In Antarctic phytoplankton, these MAAs are dominated by porphyra-334 with shinorine, mycosporine-glycine, and palythine accounting for the majority of the rest of the MAA pool (Villafañe et al., 1995; Riegger and Robinson, 1997; Ryan et al., 2002). These MAAs are used by many organisms as a chemical sunscreen for protection from UV-radiation and are thought to play a major protective role in ice algal assemblages (Arrigo and Thomas, 2004).

The marked differences between the brine and bulk ice CDOM spectra may be attributed to our sampling strategy, with sackhole brine samples integrating material from an unknown volume of sea ice depending on sackhole depth and sea ice porosity (Papadimitriou et al., 2007). The sackhole brine CDOM spectra from the present study generally represent surface and interior conditions of the sea ice, while the CDOM spectra obtained from ice cores also include bottom ice sections, which often show elevated ice algal biomass as indicated by the Chl*a* concentrations. The bottom ice sections represent sites of high *in situ* DOM production, as indicated by the higher carbon specific absorption values, and fresher, more coloured DOM. In addition, during the melting for bulk ice samples sympagic organisms are released from a higher salinity to a much lower salinity over a period of 24 h. This may result in the loss of intracellular organic compounds, although Thomas et al. (1998, 2001) have argued that these amounts will be low by comparison with the extracellular DOM pool. Nevertheless, melting represents similar conditions to those generated during seasonal ice melt, when the material in sea ice is released to the underlying water.

4.3. CDOM photo-bleaching in sea ice brine.

The photo-bleaching experiment shows that sea ice brine is susceptible to photo-bleaching of the CDOM chromophores over short time scales (i.e. days). This was evident not only in the loss of CDOM concentration, also reported by Ortega-Retuerta et al. (2010, and citations therein) in Antarctic seawater, but also in the large change in S, which has been shown to increase as photo-bleaching occurs (Vodacek et al., 1997, Moran et al., 2000). The relatively high photo-bleaching measured during the experiment may suggest that previously the DOM had little earlier exposure to UV radiation; however, Ziegler and Benner (2000) reported losses at 350 nm of 33% (May) and 81% (July) during a 35-h experiment using surface seawater, and Vodacek et al. (1997) reported a reduction of up to 70% of the CDOM absorption and fluorescence (at 355 nm) under high light conditions in surface waters of the Middle Atlantic Bight. In CDOM degradation experiments Hulatt et al. (2009) reported losses of CDOM absorption at 440 nm of up to 76% over a 16-day period in macroalgae exposed to sunlight. Although the attenuation of light through snow, ice, brine, and water in natural systems may vary from the experimental conditions, the results of Hulatt et al. (2009) indicate that PAR may be as destructive to CDOM chromophores as UVR.

The coincidental loss of DOC as reported by Osburn et al. (2009) was not evident, indicating either an decoupling of CDOM photoreactivity and DOC photo-remineralisation, or simply that any potential change in the DOC concentration was below the detection limit, occurring on the nM rather μM concentration scale. The degradation and destruction of CDOM chromophores by photobleaching seen here decreases CDOM absorption, increases the penetration of UV radiation (Moran and Zepp, 1997), and initiates the production of a suite of reactive products (Miller and Zepp, 1995; Moran and Zepp, 1997; Uher and Andreae, 1997; Stubbins et al., 2006; Kitidis et al., 2008). Of particular significance to sea ice are the detrimental effects of increased UV radiation on primary production (Arrigo and Brown, 1996), the production of biologically labile products, which may serve as a source of remineralised nutrients (Moran and Zepp, 1997), and the possible photochemical transformations of nitrate and hydrogen peroxide to hydroxyl radicals (Chu and Anastasio, 2003). Observations from snow packs have suggested that the hydroxyl radical may be linked to the production of acetaldehyde and formaldehyde (Couch et al., 2000) and that a reaction between sea ice brine and the OH radical may in part be responsible for polar ozone depletions due to liberation of gaseous halogen species (Peterson and Honrath, 2001; King et al., 2005). King et al. (2005) suggested that first-year sea ice may be an efficient medium for photochemistry, with 85% of all photochemistry occurring in the top 1 m of the ice. This may be of significant importance to the function and structure of organisms which live in this specialized habitat, particularly in young first-year sea ice as was observed during the SIPEX study.

4.4. Potential importance of sea ice-derived CDOM

The measurements from the melted ice cores suggest that, when Antarctic sea ice melts, it might represent a major source of DOM and in particular CDOM to surface waters of the seasonally ice-covered Southern Ocean. This is supported by the findings of Kieber et al. (2009) and Ortega-Retuerta et al. (2010). The effect of this material on the optical properties of the recipient oceanic waters and its importance to the local carbon budget can only be speculated on at this stage, with our data set as a starting point. Using the DOC data for bulk sea ice in Table 3, we can estimate the flux of DOC potentially released from the sea ice annually as a result of sea ice melt. Assuming an area of seasonal ice melt of 16×10^6 km^2 and an average ice thickness of 1 m (Comiso, 2010), a DOC flux of 0.5 g C m^{-2} yr^{-1} (42 mmol C m^{-2} yr^{-1}) is estimated from the melting sea ice into the surface oceanic mixed layer, which is equivalent to a total areal input of approximately 8 Tg C yr^{-1}. Although this value is low in comparison to the standing stock of DOC in Antarctic surface mixed layer [480 Tg, assuming 50 m mixed layer and average seawater DOC of 50 μmol L^{-1} (Kähler et al., 1997, Ogawa and Tanoue, 2003)], this represents a release of not only old DOC that was incorporated into the sea ice during formation, but also new and presumably more labile DOC to the surface waters. In contrast, the standing stock of DOC in the Antarctic surface mixed layer is likely to be older and more refractory. Our annual DOC input estimate of 8 Tg C from sea ice suggests that about 11% of total annual primary production by sea ice algae (70 Tg C yr^{-1}; Arrigo et al., 2010) is potentially exported to the surface oceanic waters as DOC during the seasonal sea ice melt. For comparison, Arctic river catchments export 16 Tg C to the

Arctic Ocean from a catchment area of similar size to that of the seasonal Antarctic sea ice melt zone (Raymond et al., 2007).

sea ice-derived CDOM is likely to influence the optical properties of the surface Antarctic waters and as a consequence influence primary production within these waters via either UV protection or the attenuation of visible light (Arrigo and Brown 1996), although this might be a transient feature due to the susceptibility of this material to photo-bleaching, as shown in our experiment. Ice melt will also influence the spectral characteristics of CDOM absorption in these surface waters as the material released from the ice has low S values, which equate to a flatter absorption spectrum, i.e. relatively greater absorption of visible wavelengths. Antarctic sea ice therefore represents a productive environment and a likely important source of labile DOC and fresh autochthonous CDOM to surface waters, which in turn influence microbial heterotrophic and autotrophic production, respectively, and thus play a significant role in the cycling of organic matter in the Southern Ocean.

Acknowledgments

CS was supported by the Carlsberg Foundation and the Danish Research Council (grant #272-07-0485). DNT, LN & SP were supported by grants from NERC, The Royal Society and the Leverhulme Trust. MAG was supported by a grant from the Academy of Finland (# 108150). RHK was supported by the German Research Council (DFG; grant #WE2536/6-2). The work during SIPEX was supported by the Australian Government through the Antarctic Climate and Ecosystems Cooperative Research Centre, and by the Australian Antarctic Division through AAS project 2767. We are grateful to the crews of R.V. *Polarstern* and R.S. *Aurora Australis* as well as numerous colleagues, too many to mention, on each trip for their help in making this work possible. In particular we thank H. Betts, E Allhusen, A Scheltz, D.P. Kennedy and R. Thomas for their help in sample analyses and preparation for the cruises. We also thank Lisa Miller and two anonymous reviewers for their useful suggestions on an early version of this manuscript.

References

Amon, R.M.W., Benner, R., 1996. Bacterial utilization of different size classes of dissolved organic matter. Limnology and Oceanography 41, 41–51.

Arrigo, K.R., Brown, C.W., 1996. Impact of chromophoric dissolved organic matter on UV inhibition of primary productivity in the sea. Marine Ecology Progress Series 140, 207–216.

Arrigo, K.R., Thomas, D.N., 2004. Large scale importance of sea ice biology in the Southern Ocean. Antarctic Science 16, 471–486. doi:10.1017/S0954102004002263.

Arrigo, K.R., Mock, T., Lizotte, M.P., 2010. Primary producers and sea ice. In: Thomas, D.N., Dieckmann, G.S. (Eds.), Sea Ice 2nd Edition Wiley-Blackwell, Oxford, pp. 283–325.

Belzile, C., Johannessen, S.C., Gosselin, M., Demers, S., Miller, W.L., 2000. Ultraviolet attenuation by dissolved and particulate constituents of first-year ice during late spring in an Arctic polynya. Limnology and Oceanography 45, 1265–1273.

Belzile, C., Guo, L., 2006. Optical properties of low molecular weight and colloidal organic matter: Application of the ultrafiltration permeation model to DOM absorption and fluorescence. Marine Chemistry 98, 183–196.

Benner, R., Louchouarn, P., Amon, R.M.W., 2005. Terrigenous dissolved organic matter in the Arctic Ocean and its transport to surface and deep waters of the North Atlantic. Global Geochemical Cycles 19, GB2025. doi:10.1029/2004GB002398.

Blough, N.V., Green, S.A., 1995. Spectroscopic characterization and remote sensing of nonliving organic matter. In: Zepp, R.G., Sonntag, C. (Eds.), The Role of Nonliving Organic Matter in the Earth's Carbon Cycle.. John Wiley and Sons, pp. 23–45.

Blough, N.V., Del Vecchio, R., 2002. Chromophoric DOM in the coastal environment. In: Hansell, D.A., Carlson, C.A. (Eds.), Biogeochemistry of Marine Dissolved Organic Matter. Academic Press, London, pp. 509–546.

Bricaud, A., Morel, A., Prieur, L., 1981. Absorption by dissolved organic matter of the sea (yellow substance) in the UV and visible domains. Limnology and Oceanography 26, 43–53.

Carder, K.L., Steward, R.G., Harvey, G.R., Ortner, P.B., 1989. Marine humic and fluvic acids: Their effects on remote sensing of ocean chlorophyll. Limnology and Oceanography 34, 68–81.

Chin, Y.-P., Gschwend, P.M., 1992. Partitioning of polycyclic aromatic hydrocarbons to marine porewater organic colloids. Environmental Science and Technology 26, 1621–1626. doi:10.1021/es00032a020.

Chu, L., Anastasio, C., 2003. Quantum yields of hydroxyl radical and nitrogen dioxide from the photolysis of nitrate on ice. Journal of Physical Chemistry A 107, 9594–9602. doi:10.1021/jp0349132.

Coble, P.G., 2007. Marine optical biogeochemistry: The chemistry of ocean color. Chemical Reviews 107, 402-418, 10.1021/cr050350+.

Comiso, J.C., 2010. Variability and trends of the global sea ice cover. In: Thomas, D.N., Dieckmann, G.S. (Eds.), Sea Ice 2nd Edition Wiley-Blackwell, Oxford, pp. 205–246.

Couch, T.L., Sumner, A.L., Dassau, T.M., Shepson, P.B., Honrath, R.E., 2000. An investigation of the interaction of carbonyl compounds with the snowpack. Geophysical Research Letters 27, 2241–2244.

Cox, G.F.N., Weeks, W.F., 1983. Equations for determining the gas and brine volumes in sea ice samples. Journal of Glaciology 29, 306–316.

Davidson, A.T., Bramich, D., Marchant, H.J., McMinn, A., 1994. Effects of UV-B irradiation on growth and survival of Antarctic marine diatoms. Marine Biology 119, 507–515.

Dumont, I., Schoemann, V., Lannuzel, D., Chou, L., Tison, J.-L., Becquevort, S., 2009. Distribution and characterization of dissolved and particulate organic matter in Antarctic pack ice. Polar Biology 32, 733–750.

Ehn, J., Granskog, M.A., Reinart, A., Erm, A., 2004. Optical properties of melting landfast sea ice and underlying seawater in Santala Bay, Gulf of Finland. Journal of Geophysical Research 109, C09003. doi:10.1029/2003JC002042.

Eicken, H., Lange, M.A., Dieckmann, G.S., 1991. Spatial variability of sea ice properties in the northwestern Weddell Sea. Journal of Geophysical Research—Oceans 96 (C6), 10603–10615.

Ertel, J.R., Hedges, J.I., Devol, A.H., Richey, J.E., de Nazaré Góes Ribeiro, M., 1986. Dissolved humic substances of the Amazon River system. Limnology and Oceanography 31, 739–754.

Evans, C.A., O'Reilly, J.E., Thomas, J.P., 1987. A Handbook for the Measurement of Chlorophyll a and Primary Production. Biological Investigations of Marine Antarctic Systems and Stocks (BIOMASS). Texas A & M University.

Fritsen, C.H., Wirthlin, E.D., Momberg, D., Lewis, M.J., Ackley, S.F., 2011. Bio-optical properties of Antarctic pack ice in the early austral spring. Deep-Sea Research II 58 (9–10), 1052–1061.

Garrison, D.L., Close, A.R., 1993. Winter ecology of the sea ice biota in Weddell Sea pack ice. Marine Ecology Progress Series 96, 17–31.

Gleitz, M., Rutgers v.d. Loeff, M., Thomas, D.N., Dieckmann, G.S., Millero, F.J., 1995. Comparison of summer and winter inorganic carbon, oxygen and nutrient concentrations in Antarctic sea ice brine. Marine Chemistry 51, 81–91.

Granskog, M.A., Kaartokallio, H., Thomas, D.N., Kuosa, H., 2005. Influence of freshwater inflow on the inorganic nutrient and dissolved organic matter within coastal sea ice and the underlying waters in the Gulf of Finland (Baltic Sea). Estuarine Coastal and Shelf Science 65, 109–122.

Granskog, M., Kaartokallio, H., Kuosa, H., Thomas, D.N., Vainio, J., 2006. Sea ice in the Baltic: A review. Estuarine Coastal and Shelf Science 70, 145–160.

Haas, C., Nicolaus, M., Batzke, A., Willmes, S., Lobach, J., 2007. Changes of sea ice physical properties during the onset of melt. ISPOL Cruise Report. Reports in Polar Research 551 571–102.

Haas, C., Friedrich, A., Li, Z., Nicolaus, M., Pfaffling, A., Toyota, T., 2009. Regional variability of sea ice properties and thickness in the northwestern Weddell Sea obtained by *in-situ* and satellite measurements. Cruise Report Winter Weddell Outflow Study (WWOS)-ANT XXIII/7. Reports in Polar Research 586, 36–74.

Hellmer, H.H., Schröder, M., Haas, C., Dieckmann, G.S., Spindler, M., 2008. The ISPOL drift experiment. Deep-Sea Research II 55, 913–917.

Hellmer, H., van Caspel, M., Macrander, A., Olbers, D., Sellmann, L., Mata, M., Da Silva Duarte, V., Kerr Duarte Perreira, R., Nuez, N., Schodlok, M., 2009. Water mass variability in the north-western Weddell Sea: A continuation of the DOVETAIL project. Reports in Polar Research 586, 16–21.

Herborg, L.-M., Thomas, D.N., Kennedy, H., Haas, C., Dieckmann, G.S., 2001. Dissolved carbohydrates in Antarctic sea ice. Antarctic Science 13, 119–125.

Holm-Hansen, O., Lorenzen, C.J., Holmes, R.W., Strickland, J.D.H., 1965. Fluorometric determination of chlorophyll. ICES Journal of Marine Science (International Council for the Exploration of the Sea) 30, 3–15.

Hulatt, C.J., Thomas, D.N., Bowers, D.G., Norman, L., Zhang, C., 2009. Exudation and decomposition of chromophoric dissolved organic matter (CDOM) from some temperate macroalgae. Estuarine Coastal and Shelf Science 84, 147–153.

Kähler, P., Bjørnsen, P.K., Lochte, K., Antia, A., 1997. Dissolved organic matter and its utilization by bacteria during spring in the Southern Ocean. Deep-Sea Research II 44, 341–353.

Karentz, D., McEuen, F.S., Land, M.C., Dunlop, W.C., 1991. Survey of mycosporine-like amino acid compounds in Antarctic marine organisms: Potential protection from ultraviolet exposure. Marine Biology 108, 157–166.

Kattner, G., Thomas, D.N., Haas, C., Kennedy, H., Dieckmann, D.S., 2004. Surface ice and gap layers in Antarctic sea ice: highly productive habitats. Marine Ecology Progress Series 277, 1–12.

Kennedy, H., Thomas, D.N., Kattner, G., Haas, C., Dieckmann, G.S., 2002. Particulate organic matter in Antarctic summer sea ice: concentration and stable isotopic composition. Marine Ecology Progress Series 238, 1–13.

Kieber, D.J., Toole, D.A., Kiene, R.P., 2009. Chromophoric dissolved organic matter cycling during a Ross Sea *Phaeocystis Antarctica* bloom. In: Krupnik, I., Lang, M.A., Miller, S.E. (Eds.), Smithsonian at the Poles: Contributions to International Polar Year Science – a Smithsonian Contribution to Knowledge. Smithsonian Institute Scholarly Press, Washington, D.C, pp. 319–333.

King, M.D., France, J.L., Fisher, F.N., Beine, H.J., 2005. Measurement and modeling of UV radiation penetration and photolysis rate of nitrate and hydrogen peroxide in Antarctic sea ice: An estimate of the production rate of hydroxyl radicals in first-year sea ice. Journal of Photochemistry and Photobiology A: Chemistry 176, 39–49.

Kitidis, V., Uher, G., Woodward, E.M.S., Owens, N.J.P., Upstill-Goddard, R.C., 2008. Photochemical production and consumption of ammonium in a temperate river-sea system. Marine Chemistry 112, 118–127.

Lannuzel, D., Schoemann, V., de Jong, J., Tison, J.-L., Chou, L., 2007. Distribution and biogeochemical behaviour of iron in the East Antarctic sea ice. Marine Chemistry 106, 18–32.

Lannuzel, D., Schoemann, V., de Jong, J., Chou, L., Delille, B., Becquevort, S., Tison, J.-L., 2008. Iron study during a time series in the western Weddell pack ice. Marine Chemistry 108, 85–95.

Lemke, P., 2009. Itinerary and Summary. Cruise Report Winter Weddell Outflow Study (WWOS)-ANT XXIII/7. Reports in Polar Research 586, 10–11.

Leppäranta, M., Manninen, T., 1988. The brine and gas content of sea ice with attention to low salinities and high temperatures. Finnish Institute Marine Research Internal Report 88-2. Helsinki.

Meiners, K.M., Papadimitriou, S., Thomas, D.N., Norman, L., Dieckmann, G.S., 2009. Biogeochemical conditions and ice algal photosynthetic parameters in Weddell Sea ice during early spring. Polar Biology 32, 1055–1065. doi:10.1007/s00300-009-0605-6.

Miller, W.L., Zepp, R.G., 1995. Photochemical production of dissolved inorganic carbon from terrestrial organic matter: Significance to the oceanic organic carbon cycle. Geophysical Research Letters 22, 417–420.

Millero, F.J., Poisson, A., 1981. International one-atmosphere equation of state of seawater. Deep-Sea Research 28A, 625–629.

Moran, M.A., Zepp, R.G., 1997. Role of photoreactions in the formation of biologically labile compounds from dissolved organic matter. Limnology and Oceanography 42, 1307–1316.

Moran, M.A., Sheldon, W.M., Zepp, R.G., 2000. Carbon loss and optical property changes during long-term photochemical and biological degradation of estuarine dissolved organic matter. Limnology and Oceanography 45, 1254–1264.

Nakamura, H., Kobayashi, J., Hirata, Y., 1982. Separation of mycosporine-like amino acids in marine organisms using reversed-phase high-performance liquid chromatography. Journal of Chromatography 250, 113–118.

Nelson, N.B., Siegel, D.A., 2002. Chromophoric DOM in the open ocean. In: Hansell, D.A., Carlson, C.A. (Eds.), Biogeochemistry of Marine Dissolved Organic Matter. Academic Press, London, pp. 547–578.

Obernosterer, I., Benner, R., 2004. Competition between biological and photochemical processes in the mineralization of dissolved organic carbon. Limnology and Oceanography 49, 117–124.

Ogawa, H., Tanoue, E., 2003. Dissolved organic matter in oceanic waters. Journal of Oceanography 59, 129–147.

Ortega-Retuerta, E., Reche, I., Pulido-Villena, E., Agustí, S., Duarte, C.M., 2010. Distribution and photoreactivity of chromophoric dissolved organic matter in the Antarctic Peninsula (Southern Ocean). Marine Chemistry 118, 129–139. doi:10.1016/j.marchem.2009.11.008.

Osburn, C.L., Retamal, L., Vincent, W.F., 2009. Photoreactivity of chromophoric dissolved organic matter transported by the Mackenzie River to the Beaufort Sea. Marine Chemistry 115, 10–20.

Papadimitriou, S., Thomas, D.N., Kennedy, H., Haas, C., Kuosa, H., Krell, A., Dieckmann, G.S., 2007. Biogeochemical composition of natural sea ice brines from the Weddell Sea during early austral summer. Limnology and Oceanography 52, 1809–1823.

Papadimitriou, S., Thomas, D.N., Kennedy, H., Kuosa, H., Dieckmann, G.S., 2009. Inorganic carbon removal and isotopic enrichment in Antarctic sea ice gap layers during early austral summer. Marine Ecology Progress Series 386, 15–27. doi:10.3354/meps08049.

Patsayeva, S., Reuter, R., Thomas, D.N., 2004. Fluorescence of dissolved organic matter in seawater at low temperatures and during ice formation. EARSeL eProceedings 3, 227–238.

Perovich, D.K., Roesler, C.S., Pegau, W.S., 1998. Variability in Arctic sea ice optical properties. Journal of Geophysical Research 103, 1193–1208.

Peterson, M.C., Honrath, R.E., 2001. Observations of rapid photochemical destruction of ozone in snowpack interstitial air. Geophysical Research Letters 28 551–514.

Petrich, C., Eicken, H., 2010. Growth, structure and properties of sea ice. In: Thomas, D.N., Dieckmann, G.S. (Eds.), Sea ice 2nd Edition Wiley-Blackwell, Oxford, pp. 23–77.

Raymond, P.A., McClelland, J.W., Holmes, R.M., Zhulidov, A.V., Mull, K., Peterson, B.J., Striegl, R.G., Aiken, G.R., Gurtovaya, T.Y., 2007. Flux and age of dissolved organic carbon exported to the Arctic Ocean: A carbon isotopic study of the five largest arctic rivers. Global Biogeochemical Cycles 21, GB4011. doi:10.1029/2007GB002934.

Retamal, L., Vincent, W.F., Martineau, C., Osburn, C.L., 2007. Comparison of the optical properties of dissolved organic matter in two river-influenced coastal regions of the Canadian Arctic. Estuarine, Coastal and Shelf Science 72, 261–272.

Ricker, W.E., 1973. Linear regressions in fishery research. Journal of the Fisheries Research Board Canada 30, 409–434.

Riegger, L., Robinson, D., 1997. Photoinduction of UV-absorbing compounds in Antarctic diatoms and *Phaeocystis Antarctica*. Marine Ecology Progress Series 160, 13–25.

Ryan, K.G., McMinn, A., Mitchell, K.A., Trenerry, L., 2002. Mycosporine-like amino acids in Antarctic sea ice algae, and their response to UVB radiation. Zeitschrift für Naturforschung 57, 471–477.

Scully, N.M., Miller, W.L., 2000. Spatial and temporal dynamics of colored dissolved organic matter in the North Water Polynya. Geophysical Research Letters 27, 1009–1011.

Shick, J.M., Dunlap, W.C., Chalker, B.E., Banaszak, A.T., Rosenzweig, T.K., 1992. Survey of ultraviolet radiation-absorbing mycosporine-like amino acids in organs of coral reef holothuroids. Marine Ecology Progress Series 90, 139–148.

Stedmon, C.A., Markager, S., Kaas, H., 2000. Optical properties and signatures of chromophoric dissolved organic matter (CDOM) in Danish coastal waters. Estuarine Coastal and Shelf Science 51, 267–278.

Stedmon, C.A., Markager, S., 2001. The optics of chromophoric dissolved organic matter (CDOM) in the Greenland Sea: An algorithm for differentiation between marine and terrestrially derived organic matter. Limnology and Oceanography 46, 2087–2093.

Stedmon, C.A., Thomas, D.N., Granskog, M., Kaartokallio, H., Papadimitriou, S., Kuosa, H., 2007. Characteristics of dissolved organic matter in Baltic coastal sea ice: Allochthonous or autochthonous origins? Environmental Science and Technology 41 7273–7279. doi:10.1021/es071210f.

Steinberg, D.K., Nelson, N.B., Carlson, C.A., Prusak, A.C., 2004. Production of chromophoric dissolved organic matter (CDOM) in the open ocean by zooplankton and the colonial cyanobacterium *Trichodesmium* spp. Marine Ecology Progress Series 267, 45–56.

Stubbins, A., Uher, G., Law, C.S., Mopper, K., Robinson, C., Upstill-Goddard, R.C., 2006. Open-ocean carbon monoxide photoproduction. Deep-Sea Research II 53, 1695–1705.

Thomas, D.N., Lara, R.J., Haas, C., Schnack-Schiel, S.B., Dieckmann, G.S., Kattner, G., Nöthig, E.-M., Mizdalski, E., 1998. Biological soup within decaying summer sea ice in the Amundsen Sea, Antarctica. In: Lizotte, M.P., Arrigo, K.R. (Eds.), Antarctic Sea Ice Biological Processes, Interactions, and Variability, 73. American Geophysical Union. Antarctic Research Series, pp. 161–171.

Thomas, D.N., Kattner, G., Engbrodt, R., Giannelli, V., Kennedy, H., Haas, C., Dieckmann, G.S., 2001. Dissolved organic matter in Antarctic sea ice. Annals of Glaciology 33, 297–303.

Thomas, D.N., Dieckmann, G.S., 2002a. Antarctic sea ice – a habitat for extremophiles. Science 295, 641–644.

Thomas, D.N., Dieckmann, G.S., 2002b. Biogeochemistry of Antarctic sea ice. Oceanography and Marine Biology: An Annual Review 40, 143–169.

Thomas, D.N., Papadimitriou, S., Michel, C., 2010. Biogeochemisry of sea ice. In: Thomas, D.N., Dieckmann, G.S. (Eds.), Sea ice 2nd Edition Wiley-Blackwell, Oxford, pp. 425–467.

Thurman, M.E., 1985. Organic Geochemistry of Natural Waters. Kluwer Academic Publishers.

Uher, G., Andreae, M.O., 1997. Photochemical production of carbonyl sulfide in North Sea water: A process study. Limnology and Oceanography 42, 432–442.

Uusikivi, J., Vähätalo, A., Granskog, M.A., Sommaruga, R., 2010. Contribution of mycosporine-like amino acids, colored dissolved and particulate matter on sea ice optical properties and ultraviolet attenuation. Limnology and Oceanography 55, 703–713.

van der Merwe, P.C., Lannuzel, D., Mancuso Nichols, C.A., Meiners, K., Heil, P., Norman, L., Thomas, D.N., Bowie, A.R., 2009. Biogeochemical observations during the winter-spring transition in East Antarctic sea ice: evidence of iron and exopolysaccharide controls. Marine Chemistry 115, 163–175 doi:10.1016/j.marchem.2009.08.001.

Villafañe, V.E., Helbling, E.W., Holm-Hansen, O., Chalker, B.E., 1995. Acclimatization of Antarctic natural phytoplankton assemblages when exposed to solar ultraviolet radiation. Journal of Plankton Research 17, 2295–2306.

Vodacek, A., Blough, N.V., DeGrandpre, M.D., Peltzer, E.T., Nelson, R.K., 1997. Seasonal variation of CDOM and DOC in the Middle Atlantic Bight: Terrestrial inputs and photooxidation. Limnology and Oceanography 42, 674–686.

Wedborg, M., Hoppema, M., Skoog, A., 1998. On the relation between organic and inorganic carbon in the Weddell Sea. Journal of Marine Systems 17, 59–76.

Weissenberger, J., 1992. The environmental conditions in the brine channels of Antarctic sea ice. Reports on Polar Research 111, 1–159.

Wozniak, B., Dera, J., 2007. Light Absorption in Sea Water.. Springer, New York.

Xie, H., Bélanger, S., Demers, S., Vincent, W.F., Papakyriakou, T.N., 2009. Photobiogeochemical cycling of carbon monoxide in the southeastern Beaufort Sea in spring and autumn. Limnology and Oceanography 54, 234–249.

Ziegler, S., Benner, R., 2000. Effects of solar radiation on dissolved organic matter in a subtropical seagrass meadow. Limnology and Oceanography 45 (2), 257–266.